

LUNAR ELEMENTAL ANALYSIS OBTAINED FROM THE APOLLO GAMMA-
RAY AND X-RAY REMOTE SENSING EXPERIMENT

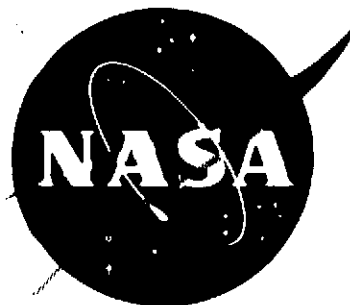
J. I. TROMBKA, J. R. ARNOLD, I. ADLER, A. E. METZGER AND
R. C. REEDY

224

A Preprint of a Manuscript from

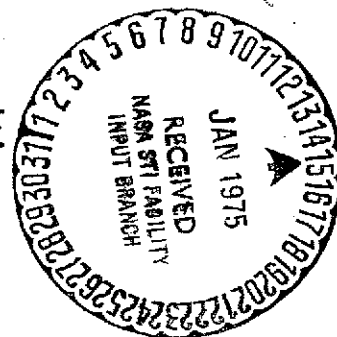
THE PROCEEDINGS OF THE SOVIET-AMERICAN CONFERENCE
ON THE COSMOCHEMISTRY OF THE MOON AND PLANETS

HELD IN MOSCOW, USSR, ON JUNE 4-8, 1974



Distributed by

THE LUNAR SCIENCE INSTITUTE
HOUSTON, TEXAS 77058



TO MAKE THE INFORMATION CONTAINED HEREIN AS WIDELY AND AS RAPIDLY
AVAILABLE TO THE SCIENTIFIC COMMUNITY AS POSSIBLE. NASA EXPECTS TO
PUBLISH THE ENGLISH-LANGUAGE VERSION OF THE PROCEEDINGS IN LATE
1975. THE FINAL TEXT MAY INCLUDE MINOR EDITORIAL CHANGES IN FORMAT, etc.

JOHN H. POMEROY, NASA HEADQUARTERS
TECHNICAL EDITOR

(NASA-TM-X-72195) LUNAR ELEMENTAL
ANALYSIS OBTAINED FROM THE APOLLO
GAMMA-RAY AND X-RAY REMOTE SENSING
EXPERIMENT (NASA) 75 p HC \$4.25
N75-14691
Unclas
CSCL 03B G3/91 07479

LUNAR ELEMENTAL ANALYSIS OBTAINED FROM THE APOLLO
GAMMA-RAY AND X-RAY REMOTE SENSING EXPERIMENT

J. I. Trombka
Goddard Space Flight Center
Greenbelt, Maryland

J. R. Arnold
University of California, San Diego
La Jolla, California

I. Adler
University of Maryland
College Park, Maryland

A. E. Metzger
Jet Propulsion Laboratory
Pasadena, California

and

R. C. Reedy
Los Alamos Scientific Laboratory
Los Alamos, New Mexico

GODDARD SPACE FLIGHT CENTER
Greenbelt, Maryland

LUNAR ELEMENTAL ANALYSIS OBTAINED FROM THE APOLLO
GAMMA-RAY AND X-RAY REMOTE SENSING EXPERIMENT

By

J. I. Trombka
Goddard Space Flight Center
Greenbelt, Maryland

J. R. Arnold
University of California, San Diego
La Jolla, California

I. Adler
University of Maryland
College Park, Maryland

A. E. Metzger
Jet Propulsion Laboratory
Pasadena, California

and

R. C. Reedy
Los Alamos Scientific Laboratory
Los Alamos, New Mexico

ABSTRACT

Gamma-ray and X-ray spectrometers carried in the Service Module of the Apollo-15 and -16 spacecraft were employed for compositional mapping of the lunar surface. The measurements involved the observation of the intensity and characteristic energy distribution of gamma rays and X-rays emitted from the lunar surface. A large scale compositional map of over 10 percent of the lunar surface was obtained from an analysis of the observed spectra. The Apollo-15 flight was at

a lunar orbital inclination of 29 degrees as compared to 9-degree inclination of the Apollo-16 flight, thus the projected ground track of the Apollo-15 flight covered a larger projected surface area than the Apollo-16 flight.

The objective of the X-ray experiment was to measure the K spectral lines from Mg, Al, and Si. Spectra were obtained and the data were reduced to Al/Si and Mg/Si intensity ratios and ultimately to chemical ratios. Analyses of the results have indicated (1) that the Al/Si ratios are highest in the lunar highlands and considerably lower in the maria, and (2) the Mg/Si concentrations generally show the opposite relationship. There is a tendency for the Al/Si values to increase from the western mare areas to the eastern limb highlands. There are distinct chemical contrasts between such features as the small mare basins and the highland rims.

The objective of the gamma-ray experiment was to measure the natural and cosmic-ray induced activity emission spectrum. At this time, the elemental abundances for Th, U, K, Fe, Ti, Si, and O have been determined over a number of major lunar regions. Regions of relatively high, natural radioactivity were found in the Mare Imbrium and Oceanus Procellarum regions. High spots of natural radioactivity were also found south of Fra Mauro, somewhat southwest of Archimedes, and south

of Aristarchus. An enhanced region of natural radioactivity was found around Van de Graaf on the far side of the moon. In regions other than Mare Imbrium and Oceanus Procellarum, an anti-correlation between natural radioactivity and lunar elevation, as determined from the Apollo laser altimeter, has been found.

From the combined results of the gamma-ray and X-ray spectrometer experiments almost complete information concerning the major element composition of over 10 percent of the lunar surface has been obtained. Distributions have also been mapped for K, Th, and Ti. Interesting correlations between lunar topography and magnetic and gravitational properties have been found.

LUNAR ELEMENTAL ANALYSIS OBTAINED FROM THE APOLLO GAMMA-RAY AND X-RAY REMOTE SENSING EXPERIMENT

By

J. I. Trombka
Goddard Space Flight Center
Greenbelt, Maryland

J. R. Arnold
University of California, San Diego
La Jolla, California

I. Adler
University of Maryland
College Park, Maryland

A. E. Metzger
Jet Propulsion Laboratory
Pasadena, California

and

R. C. Reedy
Los Alamos Scientific Laboratory
Los Alamos, New Mexico

INTRODUCTION

Gamma-ray and X-ray fluorescent spectrometers carried in the Service Module of the Apollo-15 and Apollo-16 spacecraft were employed for compositional mapping of the lunar surface. The measurements involve the observation of the intensity and characteristic energy distribution of gamma rays and X-rays emitted from the lunar surface. The objective of the X-ray experiment was to measure the K spectral lines from Mg, Al, and Si, while that of the gamma-

ray experiment was to measure the natural and cosmic-ray induced emission spectrum. At this time it is possible to obtain large scale compositional maps of over 10 percent of the lunar surface for Al, Mg, Th and U, K, Fe, Ti, Si, and O. The Apollo-15 flight was at a lunar orbital inclination of about 29 degrees as compared to about a 9-degree inclination of the Apollo-16 flight; thus, the projected ground track of the Apollo-15 flight covered a larger surface area than the Apollo-16 flight.

Over the past two years, certain results of these Apollo gamma-ray and X-ray remote sensing experiments have appeared in the literature. This report will present a summary of the results and indicate the present methods employed in the analysis of the data. It is hoped that this summary of both the analytic methods and results will enable other investigators in planetology to make optimum use of the results.

INSTRUMENTATION AND DATA ANALYSIS GAMMA-RAY EXPERIMENT

The gamma-ray spectrometer consisted of a 7- by 7-cm right cylindrical NaI(Tl) crystal detector with a plastic anticoincidence mantle to suppress response to charged particles and a 512-channel, pulse-height analyzer including an amplifier, but no memory. The information was transmitted event by event in real time or, if necessary, was stored on a magnetic tape for later transmission to earth.

Spectra were obtained by accumulating the pulses received on earth for various periods of time. Details of the experimental system are described in Arnold et al. (1972) and Harrington et al. (1974). The instrument was mounted on a boom capable of extending 7.6 m from the spacecraft in order to minimize background interference due to gamma-ray emission from the spacecraft.

The model on which the data analysis is based can be found in Reedy, Arnold, and Trombka (1973). The experimental data as received from the Johnson Spacecraft Center were processed for analysis by eliminating those data having parity errors and other problems and analytically shifting to a constant level of gain. (The overall instrument gain decreased over 40 percent on Apollo-15 and about 10 percent on Apollo-16 during the lunar phase of the mission.) The gain as adjusted for analysis was about 19 keV/channel. The spectra were then corrected for solid angle to a constant height of 110 km above the lunar surface. All data obtained over each region to be analyzed were then accumulated into master spectra. An initial background correction was made for the general sky background of gamma radiation, for natural gamma-ray emission, and for cosmic ray induced gamma-ray emission from the spacecraft, local mass around the detector, and the detector itself. The background level was determined from measurements made during the trans-Earth flights

of Apollo-15 and Apollo-16, returning from the moon. Shown in Figure 1 is a pulse-height spectrum obtained during trans-Earth flight.

Two types of data analyses were carried out: (1) integral counts in the ~ 0.6 - to ~ 2.7 -MeV region were used to determine the variation of the counts due to the natural emitters K, U, and Th, and (2) detailed spectral analysis was performed to separate the elemental components enabling quantitative analyses to be obtained for Th + U, K, Fe, Ti, Mg, Si and O. Using the methods described in Reedy, Arnold, and Trombka (1973), a minimum of 30 to 40 minutes of counting were required for these quantitative analyses; for smaller data blocks statistical errors produce unacceptable scatter. Much shorter time periods of data were used with the integral counting method for determining the natural radioactivity distribution. This integral count method works well in determining natural radioactivity. It was found that for the most part the variation in the count rate in the 0.6 - to 2.7 -MeV region can be attributed to gamma emission from K, Th, and U (Metzger et al., 1973).

The quantitative analyses were carried out using interactive matrix inversion procedures described schematically by Reedy, Arnold, and Trombka (1973). The most difficult analysis was the derivation of the lunar gamma-ray continuum: that is, the portion of the flux in the 0.5 - to 10 -MeV region which does not contain

characteristic lines. The continuum was found to produce about 85 percent of the counts in the detector. While its general shape is understood, the continuum must be derived from the data. The continuum shape and magnitude are not constant over the whole moon. Below 3 MeV, the lines due to the radioactive elements K, Th, and U make an important contribution to this continuum by Compton scattering in the lunar material. In this manner, the continuum was separated into two components: one component was found to be constant over the lunar surface while a second component varies as a function of the concentration of the radioactive elements K, Th, and U. The constant portion of the lunar background was derived from an analysis of lunar regions where the minimum natural radioactivity is found. The increase above this minimum level was then derived by taking differences between regions of higher activity and their low-activity regions. Empirical methods were developed to determine the magnitude and shape of the scatter buildup as a function of Th, U, and K concentration. Figure 2 shows the lowest magnitude background and the highest magnitude background used in the analysis of the Apollo-15 data. Figure 3 shows the measured lunar pulse-height spectrum obtained by integrating the spectrum over a number of hours of measurement, thus representing an average composition, over the Apollo-15 ground track and the derived lunar

background for this same average spectrum. The difference pulse-height spectrum corresponding to the lunar discrete line emission pulse-height spectrum is indicated in Figure 4. The various elemental components used in the matrix analysis method (Reedy, Arnold, Trombka, 1973) and the best least square fit obtained by synthesizing these elemental components with respect to the difference spectrum are also shown.

The results to be presented in this paper were obtained from an analysis of the net discrete line spectrum from Apollo-15 and Apollo-16. The background shapes were derived from the Apollo-15 data and were used for both Apollo-15 and Apollo-16. Good agreement for elemental concentration was achieved except for the Ti calculated from the high energy (n, γ) line in the overlap region of Apollo-15 and Apollo-16. The improved energy resolution of the Apollo-16 instrument and differences in proton induced activation may be responsible for the changes in the Apollo-16 versus Apollo-15 high energy portion of the background which affect the Ti calculation. Separate background continua for Apollo-16 are presently being calculated.

Some changes have been made in the procedure described by Reedy, Arnold, and Trombka (1973). It has been found useful to perform the analysis in two stages. In the first stage, only the spectrum from 5 to 9 MeV is analyzed; in this region, as can be seen in Figure 4, only Fe, O, Si, and Ti contribute significant intensity. In the second stage of analysis, the component intensities derived by matrix

inversion in stage one was subtracted from the spectrum, and the difference spectrum in the lower energy region was then analyzed using all the remaining components.

Another change in the analytical procedure involved the calculation of the iron component. Iron produces a line spectrum in the >0.8 -MeV region due to inelastic scatter of neutrons, the (n, n', γ) process and a second line spectrum in the >5 MeV region due to prompt capture of the (n, γ) process. Because of the good statistics for determining the distributions for this element, the two iron components were analyzed separately. The difference in the ratio of the number flux of the (n, γ) emission with respect to the (n, n', γ) process can be used as an indicator for the presence of strong thermal neutron absorbers (such as Gd and other rare earths). This can be done because the (n, γ) gamma-ray number flux is approximately proportional to the neutron flux near thermal energies (below 1 eV). The (n, n', γ) number flux is proportional to the fast flux (above 1 MeV). Since the rare earth group includes several large thermal neutron absorbers, their presence in large concentrations will depress the magnitude of the thermal flux without significantly perturbing the fast flux. This has been seen in the analysis under consideration here. For the other elements, such as Si, which have important lines of both types, the library spectra were combined into a single component. Thorium and

uranium were also combined into a single component; an estimate of the U based on an assumption that the abundance ratio of Th/U is 3.8. This was necessary because the uranium lines, although contributing significantly to the emission spectrum, have lines that are significantly masked by other lines in the discrete line spectrum. This masking is due to the poor energy resolution of NaI(Tl) detectors. Rather precise determination of the thorium component is possible because the 2.62-MeV emission line for this element is easily discernible in the discrete line pulse-height spectra (Figure 4).

The elements which can be usefully analyzed fall into two groups. For the natural radioactivities, K and (Th + U), the elemental concentrations can be derived from the decay schemes and the properties of the detector, using theory and laboratory calibrations, with no ambiguity in principle. Concentration values for these elements were derived in this way, without adjustable parameters. The elements that depend on cosmic-ray excitation, O, Si, Fe, Mg, and Ti, require input information from nuclear and cosmic-ray physics whose combined accuracy is not yet very high. The agreement to be expected is no better than that for the parent models as proposed by Reedy and Arnold (1972) for the production of cosmogenic nuclides in the Moon and that of Lingenfelter, Canfield, and Hampel (1972) for low energy neutrons. The depth variations of induced radioactivity observed in

the lunar soil are in rather good agreement (Finkel et al., 1974) with Reedy and Arnold's calculations, but the absolute amounts depart by ± 25 percent from calculated values from Apollo gamma-ray data. The experiment of Woolum and Burnett (1974) on Apollo 17 confirms to some extent the calculations of Lingenfelter et al. (1972) of the lunar neutron flux, but suggests a somewhat harder neutron spectrum. The deviations observed from the Reedy, Arnold, and Trombka (1973) calculations also suggest a harder neutron spectrum.

The best way to treat the data for O, Si, Fe, Mg, and Ti is to use "ground-truth" data, normalizing the orbital data to the surface samples at one or more selected points. While there are many mapped areas which include several sites from which samples have been returned, most of these are unsuitable because of local variability of the soil chemistry, as for example, the Apollo-15 landing site. The two best sites are Mare Tranquillitatis, where the Apollo-11 analyses are supplemented by the results of the Surveyor-5 experiment (Turkevich et al., 1969), and the Apollo-16 landing site near the Descartes region. The Apollo-15 and -16 spectrometer Fe, Mg, and Ti data were normalized to the ground-truth data for Mare Tranquillitatis and the Descartes region ground-truth data were used as a check. Another check was performed by comparing of regions overflowed by both Apollo-15 and Apollo-16.

Table 1 gives the ground-truth element concentrations used for the region of Mare Tranquillitatis derived the published values (see Table 1) for the soil sample 10084. The exception is Ti with a somewhat lower assumed value. The reason for this exception is that the count rates for the spectral region in which Ti is important (5.97 to 6.37 MeV) show a variation that is far outside the counting error over the Tranquillitatis region. The Apollo and Surveyor sites are in the two regions of highest observed counting rate. Because O, Si, and Fe appear to be constant in this region, the assumption is that any variation in integrated intensity is due to Ti. The conclusion drawn is that the true mean Ti concentration over the region is lower by a factor of 0.65 than that observed on the ground; this correction of course increases the uncertainty of the Ti values.

In the work to be reported, errors are not quoted because, in complex interactive analyses of the present type, the magnitude of random and systematic errors are difficult to evaluate. The main sources of error are (1) statistical counting errors, (2) the uncertainties in the shape of the subtracted continuum, (3) unknown interactions between components, and (4) where applicable, the ground-truth normalization. At the present stage of analysis, the ground-truth comparisons and comparisons on the overlap regions of Apollo-15 and -16 give an indication of the uncertainties.

Finally, with regard for the data analysis, the compositions determined reflect the average composition down to about 20 cm in depth.

Table 1
Ground-Truth Values
Mare Tranquillitatis

O	40.8%
Si	19.6%
Fe	12.1%
Mg	4.8%
Ti	2.9%*
Th	2.1 ppm
K	1100 ppm

All data in this and later tables are in % or ppm element by weight. The values of Th and K are given for convenience; they are not used for re-normalization. The data are for soil 10084 (Wakita et al., 1970; Schonfeld and Meyer, 1972).

* This is 0.65 times the soil 10084 concentration. See text for discussion.

THE X-RAY EXPERIMENT

The X-ray spectrometer consists of three large-area proportional detectors; a set of large-area filters for energy discrimination among the characteristic X-rays of Al, Si, and Mg; collimators; and data-handling electronics for obtaining eight-channel pulse-height spectra.

These three detectors pointed at the lunar surface while taking measurements. A fourth proportional counter that looked in the direction opposite to the three large-area proportional counters was used as a solar monitor. The three proportional counters used to monitor the lunar X-ray flux were identical, each having an effective window area of $\sim 21 \text{ cm}^2$. The window consisted of 0.0025-cm-thick Be. The proportional counters were filled to a pressure of 1 atm with the standard P-10 mixture of 90 percent argon (A), 9.5 percent carbon dioxide (CO_2), and 0.5 percent helium (He). To change the energy response, filters were mounted across the Be window aperture on two of the proportional counters. The filters consisted of a Mg foil ($5.08 \times 10^{-4} \text{ cm}$ thick) and an Al foil ($1.27 \times 10^{-3} \text{ cm}$ thick). The collimator consisted of multicellular baffles that defined a field-of-view of the three detectors to ~ 44 degrees full width at half maximum. Details of the systems can be found in Adler et al. (1972d).

In the X-ray fluorescence experiment, the production of characteristic X-rays followed the interaction of solar X-rays with the lunar surface. The typical solar X-ray is energetically capable of producing measurable amounts of characteristic X-ray from all the abundant elements with atomic numbers of approximately 14 (Si) or less. In the analysis of the data, the spectral characteristics and magnitude of the incident solar X-ray flux greatly affected the analysis. For a detailed

discussion of this problem see Adler et al. (1972d).

Figure 5 shows characteristic pulse-height spectra taken over Mare Crisium for the three detectors aboard Apollo-15. The spectra were normalized so that the area under the spectrum corresponding to the base detector is taken as unity. The effects of the Mg and Al filters can be seen in Figures 5b and 5c. An integral count method utilizing the characteristics of the filters was used to determine the intensity of the characteristic lines due to Mg, Al, and Si. The relative magnitude and absolute intensity of these lines depend on the magnitude and spectral quality of the incident solar spectrum, the angle of incidence of the solar flux with respect to the look direction of the X-ray detectors, the local altitude of the detectors with respect to the lunar surface, and the surface composition and physical characteristics. If the solar spectral shape is constant, it is found that the other correction factors having to do with detector-spacecraft geometry and physical characteristics of the surface material cancel out in the calculation ratios of the abundance ratios Al/Si and Mg/Si. Further, if it is assumed that the Si concentration is constant over the lunar surface sampled (an assumption supported to good accuracy by sample analyses to date), then these ratios reflect the changes in the Al and Mg concentration over the lunar surface. Actual concentrations were obtained by an approach that is both

theoretical and empirical. The theoretical calculations are based on the assumption of a quiet sun and a coronal temperature of $4 \times 10^6 \text{K}$. These conditions give an X-ray energy distribution, consisting of both a continuum and characteristic lines, that is consistent with the solar-monitor observations. The X-ray energy distribution and various soil compositions, as determined from the analysis of lunar samples, were used to calculate a relationship between Al/Si intensity ratios as a function of chemical ratios. The empirical approach involves the assumption that the soil values from the Apollo-11 site at Mare Tranquillitatis and the Luna-16 soil values from Mare Fecunditatis are ground-truth values. With these values and the theoretically calculated slopes, values of Al/Si concentrations for various parts of the lunar surface along the ground track were determined. The X-ray fluorescence experiment measured surface composition down to a depth of approximately 0.1 mm. Because of the gardening (mixing) of the lunar regolith by meteorite impact, no difference in composition is expected between the X-ray and gamma-ray experiments because of the different depths sampled.

The first results of the X-ray fluorescence experiments were used to map the ratios Al/Si and Mg/Si on a broad scale across the lunar surface. Recently attempts (Adler et al., 1973; Adler et al., 1974) have been made to prepare more detailed maps relating the

X-ray results to small lunar morphological features and to various parameters independently determined, such as photo-geologic observations, gravitational anomalies, and the electromagnetic sounder results.

Various methods of contouring have been considered. One approach which seems to be rather successful has been to perform trend surface studies of the lunar data (Adler et al., 1974; Podwysocki et al., 1974a). Surfaces described by different order polynomial expressions are fitted to the observed data by a least-square technique. The significance of the surface is tested by statistical means. A regional model surface which is shown to be statistically valid is assumed to be the proper model for the particular region. Differences between the observed values and the model values that are statistically significant are plotted as residuals and are interpreted as local anomalies with respect to the model. It must be remembered that in all of these analyses it has been assumed that Si is constant and that the variations can be attributed to changes to either Al or Mg composition.

EXPERIMENTAL RESULTS AND INTERPRETATIONS

Gamma-Ray Spectrometer

The first results available from the gamma-ray experiment concerned the distribution of the radioactive elements of Th, U, and K (Metzger et al., 1973; Trombka et al., 1973; and Proc. Fourth Lunar Sic. Conf., 1973.) In the spectral region above the 0.51-MeV line

and up to and including the highest energy line, the 2.61-MeV line due to Th, the regional differences in count rate are overwhelmingly due to the varying intensities of the lines of Th, U, and K. This is a fortunate circumstance because the statistical precision of the total count in this region (the integrated intensities from 0.55 to 2.75 MeV) is excellent, and good area resolution can thus be obtained. In the Proceedings of the Fourth Lunar Science Conference (1973) the count rate data are presented for 2- by 2-degree resolution elements on the lunar surface, which corresponds to a square approximately 60 km on edge. The data were adjusted to correspond to a nominal altitude of 100 km. Count rates in the energy range 0.55 to 2.75 MeV were obtained in the regions traversed by both Apollo-15 and -16 and were compared. The Apollo-16 average rate in this region is 4.6 percent greater than those from Apollo-15. This difference can be attributed to differences in particle radiation fluxes and differences in induced activity due to different trajectories through the earth's radiation belts on Apollo-15 as compared with Apollo-16. The main results of this portion of the analysis are presented on a 5-degree scale map in Figures 6a and 6b for the near and far sides of the Moon, respectively.

The range of the corrected counting rates is from about 73 to 94 counts per second, or about 25 percent. The standard deviation for a typical counting time of 300 seconds per 5-degree square is about 0.5 counts per second (cps) based on counting statistics alone; it is

about 1 cps for the shortest counting times used. The data from areas overflowed several times on successive passes and from regions overflowed on both missions provide good correlation.

The data obtained during observation periods allow some definite conclusions to be reached, even at the present early stage of data analysis.

(1) On both missions, all 5-degree regions within and bounding the overflowed western maria show higher levels of radioactivity than any 5-degree region elsewhere. The contrast between this region and the rest of the observed Moon is striking, particularly as it extends to a comparison with the eastern maria. It is reasonable to infer that in most instances, the western mare regions not overflowed are also highly radioactive and that other regions of the moon are generally less radioactive. With reference to the radioactive elements, the boundaries between Oceanus Procellarum and named mare regions contiguous to Oceanus Procellarum, such as Mare Nubium, do not correspond to boundaries of composition. These observations, when combined with the radioactive content found in samples from the Apollo-12 and -14 sites (Lunar Sample Prelim. Exam. Team, 1971), imply a geochemical relationship for the entire Mare Imbrium-Oceanus Procellarum Region.

(2) There is detailed structure within the high-radioactivity

region. The highest concentrations observed are in the Aristarchus area, in high ground west of the Apollo-15 landing site and south of Archimedes, and in the area south of the crater Fra Mauro. The Fra Mauro area overflowed is about 7 degrees south of the Apollo-14 landing site, soil from which showed comparable levels of radioactive concentration. The data from this area indicate that the Fra Mauro is, superficially at least, related to the western maria rather than the adjacent highlands as has sometimes been inferred from the albedo and topography.

(3) The eastern maria show evidence of having locally enhanced radioactivity which is lower than that of the western maria. Higher intensities of radioactivity, relative to the surrounding highlands, are visible in Mare Tranquillitatis, Mare Fecunditatis, Mare Crisium, and Mare Smythii. This intensity has not been seen in Mare Serenitatis, but its accessibility to ejecta from Mare Imbrium tends to "wash out" any inherent difference. From a numerical analysis, Mare Crisium shows more contrast in radioactivity relative to its surroundings than the other eastern maria observed by the Apollo spectrometers.

(4) The highland regions show low radioactivity, except on the borders of the western maria where lateral mixing seems to have occurred. On the lunar farside, the highlands to the east (180 to 90 degrees east longitude) are perceptibly more radioactive than those

of the west (90 to 180 degrees west longitude) along both the Apollo-15 and -16 ground tracks. The same is true for the limb areas (compare the highland area 60 to 105 degrees east longitude to the area 90 to 120 degrees west longitude). There is a small radioactive maximum on the lunar farside near Van de Graaff (where a major magnetic anomaly is also seen); no increase is observed at these longitudes between 8 to 10 degrees north latitude.

(5) Figure 7 shows a profile of the lunar topography observed below the Command Service Module (CSM) by the laser altimeter for single orbits of the Apollo-15 and -16 missions (Sjogren and Wollenhaupt, 1973). Superimposed on Figure 7 are points representing the relative natural radioactivity. Ignoring the region of highest radioactivity in the Mare Imbrium-Oceanus Procellarum area, a strong inverse correlation between elevation and natural radioactivity is displayed over the remaining 360-degree track. Regions of high elevation are characterized by low material radioactivity and vice versa. While this inverse relationship is observed in the Mare Imbrium-Oceanus Procellarum region, there is structure in the radioactivity which does not correlate with changes in topography. On the lunar farside, this inverse correlation extends to an observation of greater east-west asymmetry around 180 degrees for the Apollo-16 trajectory than that of Apollo-15 — an asymmetry which exists for both elevation

and natural radioactivity. This inverse correlation does not appear consistently in intercomparisons among maria but rather appears to be reflecting both the nature and extent of major lunar differentiation processes. If the Moon is in isostatic equilibrium, the more extensive the early anorthositic differentiation, as characterized by lower densities and lower concentrations of the naturally radioactive nuclides than found in mare regions, the higher the elevation and the lower the radioactivity expected.

The major lunar depression occurs in the vicinity of the crater Van de Graaff and exhibits the sharpest contrast in elevation with adjacent highlands along either ground track, that is, about 8 km. This depression is also the site of the only major farside enhancement in natural radioactivity. The depression extends some 30 degrees in longitude on either side of 180 degrees longitude, and the gamma-ray feature is of comparable extent. Figure 8 shows the Van de Graaff area in detail. The gamma-ray intensities (counts/sec) between 0.55 MeV and 2.75 MeV are calculated in 2- by 2-degree segments of area north and south of the laser altimeter track. In this case, the gamma-ray data have been corrected for spacecraft altitude but not for differences in elevation of the lunar surface. Also shown is the lunar surface magnetic field as mapped by the Apollo-15 subsatellite magnetometer with contours given in tenths of gammas (Coleman et al., 1973). The

elevation track is shown by the dotted line with variations from a mean radius of 1738 km tabulated at the top (Sjogran and Wollenhaupt, 1973). The magnetic feature shown is the strongest observed by either the Apollo-15 or -16 subsatellite magnetometers (Coleman et al., 1973). Ignoring values based on less than 50 seconds of counting time, the highest gamma-ray intensity location is identical to the minimum elevation in the Van de Graaff region. No trace of this enhanced radioactivity was found at regions north of this feature by Apollo-16. Thus, over that portion of the lunar surface scanned to date, the largest surface remanent magnetic field, one of the deepest depressions, and the only significant farside enhancement in radioactivity have all been observed within about 5 degrees (150 km) of each other. This Van de Graaff area is a notable, and to date, quite singular, exception to the general conditions prevailing on the lunar farside and, when understood, is likely to contribute significantly to an understanding of lunar evolutionary processes. This will be considered further after the following discussion of elemental composition maps.

Because of statistical problems in performing the detailed chemical analyses, the mission ground track was divided into a series of regions. Table 2 gives the number, assigned name, and lunar coordinates for each region. Figure 9 shows the actual regions in outline form. In the case of Apollo-15, the data for early revolutions have not been used in this synthesis; hence, the western portion (south-

Table 2
Lunar Regions Analyzed

Number	Assigned Name	Coordinates Boundary Regions
<u>Apollo-15:</u>		
34	Van de Graaff Region	168°W-168°E
35	Highland East Farside	168°E-82°E(south of 10°S) 168°E-88°E(north of 10°S)
36	Highland East Nearside	from (Region 35) to 60°E
37	Mare Fecunditatis	60°E-42°E
38	Mare Tranquillitatis	42°E-21°E
39	Mare Serenitatis	21°E-6°E
40	Archimedes Region	6°E-15°W
41	Mare Imbrium	15°W-39°W
42	Aristarchus Region	39°W-54°W
43	Oceanus Procellarum (north)	54°W-81°W
44	Highland West Farside	81°W-168°W
<u>Apollo-16:</u>		
26	Highland East Farside	180°-142°E
22	Mendeleev	142°E-138°E
28	Highland East Limb	138°E-92°E
20	Mare Smythii	92°E-83°E
19	Highland East Nearside	83°E-55°E
17	Mare Fecunditatis	55°E-44°E

Table 2 (cont.)
Lunar Regions Analyzed

Number	Assigned Name	Coordinates Boundary Regions
<u>Apollo-16:</u>		
14	Intermediate Mare-Eastern Highlands	44°E-21°E
12	Highland Nearside Center	21°E-5°E
10	Ptolemaeus-Albategnius	5°E-5°W
23	Fra Mauro Region	5°W-20°W
8	Mare Cognitum	20°W-30°W
5	Oceanus Procellarum (south)	30°W-50°W
3	Grimaldi Region	50°W-76°W
2	Oriente Rings	76°W-105°W
29	Highland West Limb	105°W-119°W
1	Hertzprung Region	119°W-136°W
27	Highland West Farside	136°W-180°

western or northwestern in east and west longitudes, respectively, except those near 0 and 180 degrees longitude) of regions observed by Apollo-15 are heavily weighted. These regions were chosen by considering major topographic boundaries, the density of high quality data in a given region, and the contrasts observed in the radioactivity maps (Figure 6). The smallest regions, such as Mendeleev, were chosen in order to determine the minimum area in which useful data can be derived; the errors in these regions are so large that no statistically meaningful concentrations can be derived. In this paper of the analysis only data with sufficient total counts above background, indicating significantly low statistical errors, were used; thus complex border regions were assigned to mare or highland. Doubtless, this reduced the true chemical contrasts in some regions.

Table 3 presents the results of the analysis for Apollo-15 data, normalizing Fe, Mg, and Ti as described above. The values for Fe are weighted means for the two modes of analysis. Starred values note regions where the values determined from neutron capture (low energy) are well below those from inelastic scatter (MeV neutrons). These regions appear to have high concentrations of K, Rare Earths, and P (KREEP), whose rare earth content should depress the thermal flux. In such places the true Fe content may be up to a few percent higher than shown here.

Table 3
Apollo-15: Element Concentrations by Regions

Region	Fe(%)	Mg(%)	Ti(%)	Th(ppm)	K(ppm)
34	7.7	3.8	0.1	2.3	1600
35	6.5	4.5	1.3	1.0	940
36	9.3	5.7	0.8	1.4	1200
37	11.3	7.0	2.2	1.2	1400
38 ^a	(12.1)	(4.8)	(2.9)	1.7	1200
39	10.7	6.6	2.6	2.3	1700
40	8.4*	6.3	0.8	6.8	3100
41	13.6	6.2	1.4	5.8	1700
42	9.6*	4.9	2.2	6.9	2500
43	10.5	4.6	2.0	3.9	1700
44	5.7	3.5	1.5	0.4	950
All data	8.7	4.8	1.45	2.2	1230

^aValues in parentheses are ground-truth data used to normalize concentrations for these elements in all regions.

*Region of apparent depressed thermal neutron flux (see text).

Table 4 gives the Apollo-16 results. The Apollo-15 continuum was used for this work, with very good consistency except for the Ti results, which are omitted. Here again, Fra Mauro gives evidence of a depressed thermal neutron flux; the apparent depression in a few highland regions is not yet understood.

Table 4
Apollo-16: Element Concentrations by Regions

Region	Fe(%)	Mg(%)	Th(ppm)	K(ppm)
26	6.2	3.4	0.6	920
22	4.3	3.0	0.5	960
28	7.2	2.9	0.5	840
20	8.8	2.8	1.3	1900
19	8.6	4.5	1.3	980
17	9.0	4.6	2.1	1100
14	9.0	3.5	1.5	1300
12	5.9	4.0	2.1	1400
10	4.8*	5.2	5.0	2700
23	9.7*	5.7	10.5	3900
8	12.1	4.9	8.4	3600
5	12.2	5.0	5.0	2300
3	4.4*	3.6	2.4	1100
2	4.7	2.9	0.8	1000
29	3.5*	2.1	0.4	1200
1	3.6*	3.6	0.6	720
27	5.2	2.7	0.5	730
All data	7.2	3.6	2.1	1300

*Region of apparent depressed thermal neutron flux (see text).

In Table 5 a number of instructive comparisons are presented. In the cross-over region near the east limb, the regions analyzed on the two missions are roughly the same, and the comparison should give good agreement. The highland region from 5 to 21 degrees east longitude, which includes the Descartes region, is compared with the soil analysis. The deviations seen are in the expected direction if more mare and KREEP material are mixed in near the margins of the region.

There are two landing sites that were not overflowed where a plausible comparison is possible. Apollo-14 observed the northern end of the Fra Mauro formation; Apollo-16 overflowed the southern end. Whatever the origin of this feature, similarities are to be expected throughout. Apollo-12 sampled an area of Oceanus Procellarum not very far from, and topographically similar to, the area overflowed by Apollo-16. These comparisons are shown in parts (c) and (d) of Table 5.

All these comparisons seem generally satisfactory and serve to confirm the validity of the analysis. There is room for further work in a number of areas and this is underway. However, no substantial modification of the values reported here are expected.

An implication of the results just obtained is that the contrasts between mare and highland regions are as expected nearly everywhere.

Table 5

Comparisons of Orbital Data with Returned Lunar Samples

Some Comparisons

	a. East Crossover		b. Ground Truth	
	Apollo-15 Region 36	Apollo-16 Region 19	Apollo-16 Region 12	Descartes Soil ^a
Fe(%)	9.3	8.6	5.9	4.0
Mg(%)	5.7	4.5	4.0	3.3
Th(ppm)	1.4	1.3	2.1	2.0
K(ppm)	1200	980	1400	940

Ground Analogies

	c. Fra Mauro		d. Oceanus Procellarum	
	Apollo-16 Region 23	Apollo-14 Soil ^b	Apollo-16 Region 5	Apollo-12 Soil ^c
Fe(%)	9.7	8.1	12.2	12.5
Mg(%)	5.7	5.6	5.0	6.2
Th(ppm)	10.5	11.6	5.0	7.6
K(ppm)	3900	4400	2300	2600

^aFe and Mg: Average of soil analysis, taken from five papers, Third Lunar Science Conference and PET report. K and Th from Eldridge et al. (1973).

^bFe and Mg: Average of soil analysis, taken from five papers, Third Lunar Sci. Conference, and PET report. K and Th from Eldridge et al. (1972).

^cFe and Mg: Average of analyses of bulk soil 12070 and related samples in five papers, Second Lunar Sci. Conference. K and Th from O'Kelley et al. (1971).

In the maria, Fe (and less strikingly Mg) is relatively enriched. The radioactive elements show the same pattern except for one place.

The Van de Graaff region (Table 3, Region 34) shows a chemical composition different from any thus far observed on the Moon. The major elements are highland-like, though Fe is a little high for this. The concentrations of K and Th are very similar to Mare Tranquillitatis and are typical for a mare. The Ti concentration is significantly below that of any region analyzed. Such a composition could not be formed by mixing the major components as observed elsewhere.

The most exciting possibility concerning the composition of the remarkable "granitic" rock 12013 is that Van de Graaff or some chemically similar unmapped region is its source. The K/Th ratios are compatible (O'Kelley et al., 1971) and about 5 percent of material of 12013 chemistry, added to highland soil, could produce the observed radioactivity. The major elements are also compatible, though this is not a useful check at the 5-percent level. The Van de Graaff region is very far from all the landing sites; it is thus expected that such material would be uncommon among the returned samples.

The large highland regions are not entirely uniform. Most notable is an east-west asymmetry in the lunar farside. The iron concentration is higher in the eastern regions, which are lower topographically (Sjogren and Wollenhaupt, 1973), and this effect extends to the limb and near to the mare edges. The radioactivity maps

show more detail (Figure 6). The dry basins like Mendeleev give typical highland analyses within a rather large experimental error.

The values of Ti found in the farside highlands from Apollo-15 data are unexpectedly high and are another example of inhomogeneity in broad highland areas.

There are also differences among maria and KREEP-rich regions. The variability in Ti has been well documented in the mare samples and is well displayed in the comparison of Mare Imbrium (Region 41) with Oceanus Procellarum (Region 43). The Archimedes and Aristarchus regions also differ in Ti and probably in Fe.

The most interesting element ratio is K/Th (and its assumed close correlate K/U). In both missions this ratio rises from something like 400 in the KREEP-rich regions to ratios of 1000-2000 in the highlands. Figure 10 shows plots of the two-element concentrations for the two Apollo missions (15 and 16), as a function of longitude. The errors for both elements are of course larger at the lowest concentrations, but the trend is unmistakable.

Earlier, interpretations of radioactivity maps were presented in terms of a three-component model: mare basalt, KREEP, and a low-radioactivity highland component (Metzger et al., 1973). Clearly, this preliminary model is inadequate for the detailed information now available as evidenced at Van de Graaff where material not prominently

displayed in lunar samples so far described are observed. However, no broad regions dominated by radically different chemistry (basic rocks or granites) are observed in the present analysis. If such regions exist, they lie in areas so far unmapped.

X-Ray Spectrometer

With the gamma-ray spectrometer results in mind the results of the X-ray spectrometer are summarized. (Adler et al. , 1972a; b; c; d; Adler et al. , 1973; Adler et al. , 1974; Podwysocki et al. , 1974a). These results will add Al to the elemental composition obtained with the gamma-ray spectrometer. Furthermore, much more detailed information on area distribution for both Al and Mg is obtainable because of the superior spatial resolution of the X-ray detector.

Figures 11a, 11b, 12a, and 12b show Al/Si and Mg/Si profiles along a northern and a southern track observed by the Apollo-15 mission. Figures 13a and 13b show the Al/Si profile along a track of the Apollo-16 mission. Because of the greater area covered by Apollo-15, two paths for the Apollo-15 mission are included.

The method of calculation of the Al/Si and Mg/Si concentration ratios was previously discussed, and the results are shown in Tables 6, 7, and 8. Table 6 shows the consistency in measurement between

the Apollo missions. Table 7 and Table 8 give results obtained over a number of lunar features. The results are obtained by integrating the spectra obtained over a number of passes over the same feature.

The data show some striking regularities:

(1) The Al/Si ratios are highest in the eastern limb highlands and considerably lower in the mare areas. The extreme variation is about a factor of 2, the lowest value occurring in the Imbrium basin region. The Mg/Si concentration ratios generally show the opposite relationship. If the gamma-ray results reported above for the Fe concentration are considered, it is found that Fe is high in low Al regions and the converse is also found. Also, in those regions where the Mg does remain constant, compared to the spatial resolution of the gamma-ray detector, there is good agreement between Mg/Si concentrations calculated from the X-ray and gamma-ray measurements. The Al/Si and Mg/Si chemical ratios for the highlands correspond to that for anorthositic gabbro through gabbroic anorthosites or feldspathic basalts. By contrast the chemical ratios for the mare areas correspond to the mare basalts. This result is consistent with the gamma-ray results on Fe, Th, U, and K reported above.

(2) Our early reports (while the Apollo-16 mission was in progress) of very high Al/Si ratios in the Descartes area were confirmed by the analysis of the returned lunar samples from the site. The values reported of 26.5 percent aluminum oxide agrees very well with the

estimates in Table 6. It appears reasonable from the data that some material sampled at Descartes is similar to that of the eastern limb and farside highlands. This conclusion is further justified by the fact that the Mg/Si concentration ratios for some of the returned materials is about 0.18, close to the values reported here of 0.19 to 0.05. The eastern limb highlands and farside highlands, as shown in Table 6, are about 0.16 to 0.21.

(3) In both Apollo-15 and -16 missions, the Al and Mg values derived show an inverse relationship in most instances. The inverse relationship between Al obtained from the X-ray results and Fe obtained from the gamma-ray results is even more striking.

Table 6
Comparison of Overlap Between Apollo-15
and Apollo-16 Ground Tracks

Feature ^a	Apollo 16 concentration ratio		Apollo 15 concentration ratio	
	Al/Si $\pm 1\sigma$	Mg/Si $\pm 1\sigma$	Al/Si $\pm 1\sigma$	Mg/Si $\pm 1\sigma$
Mare Fecunditatis	0.41 \pm 0.05	0.26 \pm 0.05	0.36 \pm 0.06	0.25 \pm 0.03
Mare Smythii	0.45 \pm 0.08	0.25 \pm 0.05	0.45 \pm 0.06	0.27 \pm 0.06
Langrenus area	0.48 \pm 0.07	0.27 \pm 0.06	0.48 \pm 0.11	0.24 \pm 0.06
Highlands west of Smythii	0.57 \pm 0.07	0.21 \pm 0.03	0.55 \pm 0.06	0.22 \pm 0.03
Western border of Smythii	0.58 \pm 0.08	0.22 \pm 0.04	0.52 \pm 0.06	0.22 \pm 0.06
Eastern border of Smythii	0.61 \pm 0.09	0.20 \pm 0.06	0.60 \pm 0.10	0.21 \pm 0.03

^a The overlap between corresponding areas of the Apollo 16 and 15 ground tracks is not exact, so that differences for the same area may be real.

Table 7
Concentration Ratios of Al/Si and Mg/Si
for the Various Features Overflowed During Apollo-15

Feature	Concentration ratios	
	Al/Si $\pm 1\sigma$	Mg/Si $\pm 1\sigma$
West of Diophantus and Delisle, north-east of Schröters Valley	0.26 \pm 0.13	0.21 \pm 0.06
Mare Serenitatis	0.28 \pm 0.08	0.21 \pm 0.06
Diophantus and Delisle area	0.29 \pm 0.10	0.26 \pm 0.07
Archimedes Rille area	0.29 \pm 0.08	0.19 \pm 0.05
Mare Imbrium	0.30 \pm 0.10	0.21 \pm 0.06
Mare Tranquillitatis	0.34 \pm 0.06	0.25 \pm 0.04
Mare east of Littrow (Maraldi)	0.35 \pm 0.08	0.22 \pm 0.04
Palus Putredinus	0.35 \pm 0.09	0.30 \pm 0.03
Mare Fecunditatis	0.36 \pm 0.06	0.25 \pm 0.03
Apennine Mountains	0.36 \pm 0.09	0.23 \pm 0.05
Haemus Mountains, west border of Serenitatis	0.38 \pm 0.10	0.25 \pm 0.05
Mare Crisium	0.39 \pm 0.08	0.26 \pm 0.05
Tsiolkovsky	0.39 \pm 0.11	0.18 \pm 0.02
Haemus Mountains, south-south- west of Serenitatis	0.40 \pm 0.07	0.26 \pm 0.04
Littrow area	0.42 \pm 0.10	0.25 \pm 0.06
Mare Smythii	0.45 \pm 0.06	0.27 \pm 0.06
Taruntius area, between Tranquill- itatis and Fecunditatis	0.45 \pm 0.07	0.26 \pm 0.02
Langrenus area, east of Fecunditatis to 62.5° E	0.48 \pm 0.11	0.24 \pm 0.06
Highlands between Crisium and Smythii (Mare Spumans and Mare Undarum area)	0.51 \pm 0.06	0.22 \pm 0.05
Highlands east of Fecunditatis, Kapteyn area 68-73°E 7.5-15°S	0.51 \pm 0.10	0.22 \pm 0.05
Highlands west of Crisium	0.51 \pm 0.10	0.23 \pm 0.05
Highlands east of Fecunditatis 62.5-68°E, 4-12.5°S	0.52 \pm 0.10	0.22 \pm 0.05
West border of Smythii to 4-5° out from Rim	0.52 \pm 0.06	0.22 \pm 0.03
South of Crisium, Apollonius area, to Fecunditatis, 50-60°E	0.53 \pm 0.06	0.23 \pm 0.03
East border of Crisium out to 6° from Rim	0.54 \pm 0.09	0.22 \pm 0.04
Tsiolkovsky--Rim	0.54 \pm 0.12	0.16 \pm 0.02
Highlands between Crisium and Smythii, 2.5°S 69°E, 5°S 76°E, 12°N 80°E, 10°N 83°E	0.55 \pm 0.06	0.22 \pm 0.03
Highlands west of Tsiolkovsky, 110-124°E to 9-21°S	0.57 \pm 0.11	0.19 \pm 0.04
Highland east of Fecunditatis 73-85°E, 10-19°S	0.58 \pm 0.13	0.21 \pm 0.05
South and south-west of Sklodowska, 86-101°E, 18-23°S	0.59 \pm 0.14	0.19 \pm 0.07
Pirquet, 135-145°E, 18-23°S	0.59 \pm 0.15	0.16 \pm 0.05
East border of Smythii, out to 4-5° Pasteur Hilbert highlands area	0.60 \pm 0.10	0.21 \pm 0.03
101.5-110°E, 7-18°S	0.60 \pm 0.10	0.18 \pm 0.04
Hirayama, highlands east of Smythii, 89°E 12°S, 100°E 15°S, 98°E 2°S, 103°E 5°S	0.62 \pm 0.07	0.19 \pm 0.04
Highlands around Tsiolkovsky	0.62 \pm 0.12	0.15 \pm 0.06
South part of Gagarin, 144-153°E, 21-23°S	0.65 \pm 0.24	0.14 \pm 0.05

Table 8
Concentration Ratios of Al/Si and Mg/Si
for the Various Features Overflown During Apollo-16

Feature	Concentration ratio	
	Al/Si $\pm 1\sigma$	Mg/Si $\pm 1\sigma$
Mare Cognitum	0.38 \pm 0.11	0.40 \pm 0.29
Upper part of Sea of Clouds (9° to 13° W)	.39 \pm .12	.20 \pm .05
Mare Fecunditatis (42° to 57° E)	.41 \pm .05	.26 \pm .05
South of Fra Mauro (13° to 19° W)	.45 \pm .07	.26 \pm .04
Mare Smythii (82° to 92.5° E)	.45 \pm .08	.25 \pm .05
Southern edge of Mare Tranquillitatis, Torricelli area (26° to 30° E)	.47 \pm .09	.23 \pm .05
Eastern edge of Fecunditatis, Langrenus area (57° to 64° E)	.48 \pm .07	.27 \pm .06
Ptolemaeus (4° W to 0.5° E)	.51 \pm .07	.21 \pm .04
Highlands west of Ptolemaeus to Mare Nubium (4° to 9° W)	.51 \pm .11	.25 \pm .12
Highlands west of Mare Fecunditatis (37.5° to 42° E)	.52 \pm .07	.24 \pm .05
Highlands west of Smythii (72° to 77° E)	.57 \pm .07	.21 \pm .03
Western border of Smythii (77° to 82° E)	.58 \pm .08	.22 \pm .04
Highlands east of Descartes (20.5° to 26° E)	.58 \pm .07	.21 \pm .04
South of Mare Spumans (64° to 72° E)	.58 \pm .07	.25 \pm .04
Isidorus and Capella (30° to 37.5° E)	.59 \pm .11	.21 \pm .05
Highlands west of Descartes (3° to 14° E)	.59 \pm .11	.21 \pm .05
Eastern border of Mare Smythii (92.5° to 97.5° E)	.61 \pm .09	.20 \pm .06
Far-side highlands (106° to 118° E)	.63 \pm .08	.16 \pm .05
Descartes area, highlands, Apollo 16 landing site (14° to 20.5° E)	.67 \pm .11	.19 \pm .05
East of Ptolemaeus (0.5° to 3° E)	.68 \pm .14	.28 \pm .09
Highlands (97.5° to 106° E)	.68 \pm .11	.21 \pm .05
Far-side highlands west of Mendeleev (118° to 141° E)	.71 \pm .11	.16 \pm .04

(4) There are distinct chemical contrasts between such features as the small mare basins and the highland rims (note for example the crater Tsiolkovsky in Figures 11a and 11b).

An interesting use of the data was to compare the Al/Si intensity ratios to optical albedo values. These observations are particularly significant in view of the longstanding discussions about whether these albedo differences solely represent topographic differences or also reflect compositional differences among surface materials. Early workers such as Whitaker (1965) and others recognized convincing evidence for compositional changes where sharp albedo changes occur. However, it remained for the later Surveyor, Apollo, Luna, and Lunakhod missions to provide quantitative compositional data. Chemical differences related to albedo variations were first confirmed by the alpha backscattering experiment carried on Surveyors -5, -6, and -7 (Patterson et al., 1972). The Surveyor-5 and -6 experiment data were used to analyze widely separated mare sites, and chemically similar surface materials in each site were reported. Surveyor-7 experiment, on the other hand, observed a highland site and data analysis found a significant chemical difference between that region and the two mare locations. The Surveyor results and the analyses of returned lunar samples confirmed that albedo is indeed affected by composition as well as topographic differences. The X-ray fluorescence experiments on Apollo-15 and -16 now have provided the data for correlation of regional albedo with surface composition for these selected chemical elements.

The data from both Apollo flights exhibit an excellent correspondence between Al/Si values and the optical albedo values. An example from the Apollo-16 flight is shown in Figure 14. There is positive correlation between the albedo and the Al/Si values, although the rate of change is not always similar. In the Apollo-15 data, the main anomalies were observed where an occasional small Copernican-type crater occurred and produced an abnormally high albedo value. This was considered to be due to the highly-reflective, finely divided ejecta rather than to compositional changes. A similar anomaly is noted in the Apollo-16 data around 27 degrees west longitude in a Tranquillitatis embayment north of Theophilus. Four Apollo-16 orbits are plotted. Orbits 58 and 60 show the expected decrease in Al/Si with decreasing albedo. Orbits 55 and 59 on the other hand show an occasional increase in Al/Si although the albedo decreases. This may record the existence of an old 'weathered' ray consisting of aluminum-rich, highland-derived ray material which has lost its high reflectivity. This loss is thus attributed to chemical rather than physical change.

The X-ray fluorescence experiment is particularly well suited to look at the problem of horizontal transport and particularly the question of whether or not the mare fill is highland material carried by electrostatic forces. To appreciate this, one must keep in mind that the X-ray measurements are extremely shallow. A 0.1 mm layer of

basalt or feldspar would represent effectively infinite thickness. This is equivalent to about $3 \times 10^{-4} \text{ g/cm}^2$ of material.

In a recent paper (Gold, 1973), it was proposed that horizontal transport by such mechanisms as electrostatic charging have played a large role in the formation of the flat mare basins. It is obvious that if highland material had drifted into the basins to any extent, the differences between the mare and the surrounding highlands would not be perceived. In fact, very marked differences have been found and are demonstrated. There are outstanding examples such as the crater Tsiolkovsky. The ratio of aluminum in the rim area to that of the basin is about 2:1. Further, real differences can be discerned in such relatively homogeneous sites as the Serenitatis-Tranquillitatis zones and in the Tranquillitatis basin itself. There is additional substantiation in the recent paper of Kocharov and Victorov (1974) on the results obtained by the Lunakhod 2 in the crater Le Monnier. From the analysis of returned lunar samples, it has been found that the soils in the highland regions are generally like the highland rocks; and similarly in maria regions the soils are generally like the maria rocks. Thus it seems highly unlikely that these chemical differences arise because one type of rock is more easily broken up than another or more easily transported; therefore, it is questionable whether small scale, continuous, horizontal transport has played a large role

in the formation of the flat maria basin.

Finally, short-time (8- and 16-second) X-ray fluorescence data were analyzed in order to determine their capability for mapping relatively small lunar features. Fluctuation in the solar spectral shape and variation of the look angle with spacecraft altitude make this type of analysis rather difficult, but some analysis can be performed and preliminary results have been obtained (Podwysocki et al., 1974a). Spatial mapping using trend surface analysis demonstrated that a usable signal could be abstracted from Al/Si intensity ratios compiled over short time periods. Residuals from the trend surface allowed isolation of similar areas. For details of the analytic method see Podwysocki, 1974b.

In this work a portion of Mare Serenitatis and Tranquillitatis and their adjacent highlands observed during the Apollo-15 mission were chosen. Based on the analysis of variance interpretation using trend surface analysis of 16-second Al/Si ratio data, a fourth order surface is the highest order which shows the proper level of significant improvement. Figure 15 (Podwysocki et al., 1974a) shows the derived model. Ratios are highest in the highlands to the northeast and become progressively lower toward the Mare. Low ratios are associated with the maria proper; the lowest values occur in Mare Serenitatis in the northwest portion of the mapped area. A high ratio is indicated by

the Haemus Mountains in the western part of the map. The general model conforms well to the results discussed in which the highlands have higher Al/Si intensity ratios than maria. (Figures 11, 12, and 13.)

Figure 16 (Podwysocki et al., 1974) illustrates some selected anomalies based on the residuals from the fourth order surface for the Al/Si ratio data.

Areas 10 and 11 and Area 3, representing Taurus-Littrow and Haemus highlands respectively, show quite similar Al/Si ratios. Morris and Wilhelms (1967) and Carr (1966) mapped the Haemus highlands as Imbrian age Fra Mauro formation, while the Taurus-Littrow highlands have been mapped as pre-Imbrian in age. As mentioned above, X-rays of the energy level measured during the Apollo missions have a penetration capability of 10 μ m, thus only superficial materials are mapped. Hence, it might be argued that Imbrian ejecta is being mapped in the Taurus-Littrow highlands, although it may form only a thin blanket. The crater Proclus covered in Area 21 displays considerably different Al/Si and Mg/Si ratios as compared to Area 20 ejecta material (Scott and Pohn, 1972; Wilhelms, 1972) derived from Proclus. These disparate results for materials of the same provenance may indicate stratigraphic variations within Proclus and the highlands.

Area 5, containing the crater Plinius, shows up as a distant positive anomaly from the maria materials as exemplified by Areas 4 and 6. The crater occupies an area interpreted as an impact crater (Morris and Wilhelms, 1967) in an area of relatively thin mare materials at the transition between Maria Tranquillitatis and Serenitatis. Crater excavation due to impact has most likely excavated and exposed highland material from the subsurface. Topographic data indicate that the crater was excavated to approximately 1200 meters below the mare floor. This sets a maximum limit for the mare thickness, which De Hon (1974) estimates as 500 to 600 meters in this area.

Two additional positive mare anomalies which may be of significance are Areas 7 and 2. Area 7 corresponds to a wrinkle ridge and high albedo mare material as mapped by Carr (1966). Examination of Apollo-15 metric photography indicates some features which might be interpreted as volcanic terrain or extrusive features. Both Young et al. (1973), and Hodges (1973) report possible extrusive igneous features in the same general vicinity. Low albedo Mare Serenitatis materials are typified by ratios such as those in the negative residual of Area 1. This suggests that at least two types of substantially different mare basalts are present within Mare Serenitatis. Lowman (1972) suggests that these wrinkle ridge areas may contain the final differentiation products of a large basaltic body and should contain

higher alumina concentrations. Area 2, associated with a rectilinear junction of four mare ridges forming a parallelogram, also displays a similar positive anomaly.

Positive residuals associated with Areas 17 and 18, appear to be associated with zones of the highest albedo mare materials within Mare Tranquillitatis as mapped by Wilhelms (1972). The positive residual associated with Area 13 is perplexing, for it is not associated with the Jansen craters as might be expected, but is located to their east. The only explanation for this anomaly at this time may be the concentration of ray materials as mapped by Morris and Wilhelms (1967).

CONCLUSIONS

This summary of the results, as well as interpretation of the results, obtained from the Apollo X-ray and gamma-ray spectrometer experiment data presented in this work will hopefully be helpful to investigators in the field of planetology. As can be seen from the results reported, the work is not as yet completed, but much information was obtained. There is still much to be completed in the future.

The results reported in this work represent the efforts of persons too numerous to mention here. Although unnamed, appreciation to all these individuals for their help in the development, implementation, analysis, and interpretation of results of this project is expressed.

REFERENCES

- Adler, I.; Gerard, J.; Trombka, J.; Schmadebeck, R.; et al.: 1972a, "The Apollo 15 X-Ray Fluorescence Experiment." Proceedings of the Third Lunar Science Conference, Geochim. Cosmochim. Acta, Vol. 3, David R. Criswell, ed., MIT Press (Cambridge, Mass.), 2157-2178.
- Adler, I.; Trombka, J.; Gerard, J.; Lowman, P.; Schmadebeck, R.; Blodgett, H.; Eller, E.; Yin, L.; Lamothe, R.; Gorenstein, P.; and Bjorkholm, P.: 1972b, "Apollo 15 Geochemical X-ray Fluorescence Experiment Preliminary Report." Science, 175, 436-440.
- Adler, I.; Trombka, J.; Gerald, J.; Lowman, P.; Schmadebeck, R.; Blodgett, H.; Eller, E.; Yin, L.; Lamothe, R.; Osswald, G.; Gorenstein, P.; Bjorkholm, P.; Gursky, H.; and Harris, B.: 1972c, "Apollo 16 Geochemical X-ray Fluorescence Experiment: Preliminary Report." Science, 177, 256-259.
- Adler, I.; Trombka, J.; Gerard, J.; Schmadebeck, R.; et al: 1972d, "X-Ray Fluorescence Experiment." Apollo 15 Preliminary Science Report, NASA SP-289.
- Adler, I.; Trombka, J. I.; Schmadebeck, R.; Lowman, P.; Blodgett, H.; Yin, L.; Eller, E.; Podwysocki, M.; Weidner, J. R.; Bickel, A. L.; Lum, R. K. L.; Gerard, J.; Gorenstein, P.; Bjorkholm, P.; and Harris, B.: 1973, "Results of the Apollo 15 and 16 X-ray Experiment." Proceedings of the Fourth Lunar Science Conference, Geochim. Cosmochim. Acta, Suppl. 4, Vol. 3, 2783-2791.
- Adler, I.; Podwysocki, M.; Andre, C.; Trombka, J.; and Schmadebeck, R.: 1974, "The Role of Horizontal Transport - as Evaluated from the Apollo 15 and 16 Orbital Experiments." Proceedings of the Fifth Lunar Science Conference, Geochim. Cosmochim. Acta (in press).
- Arnold, J. R.; Peterson, L. E.; Metzger, A. E.; and Trombka, J. I.: 1972, Preliminary Science Report, NASA-SP 289.
- Carr, M. H.: 1966, Geologic Map of the Mare Serenitatis Region of the Moon; U. S. Geological Survey Map I-489.

Coleman, P. F.; Lichtenstein, B. R.; Russel, C. T.; Schubert, G.; and Sharp, L. R.: 1973, "The Particles and Fields Subsatellite Magnetometer Experiment." Apollo 16 Preliminary Science Report, NASA SP-315, 23-1-13.

De Hon, R. A.: 1974, "Thickness of Mare Material in the Tranquillitatis and Nectaris Basins." Proceedings of the Fifth Lunar Science Conference, Geochim. Cosmochim. Acta, (in press).

Eldridge, J. S.; O'Kelley, G. D.; and Northcutt, K. J.: 1972, "Abundances of Primordial and Cosmogenic Nuclides in Apollo-14 Rocks and Fines." Proceedings of the Third Lunar Science Conference, Geochim. Cosmochim. Acta, Suppl. 3, Vol. 2, 1651.

Eldridge, J. S.; O'Kelley, G. D.; and Northcutt, K. J.: 1973, "Radionuclide Concentrations in Apollo 16 Samples," Proceedings of the Fourth Lunar Science Conference, Geochim. Cosmochim. Acta, Suppl. 4, Vol. 2, 2115.

Finkel, R. C.; Imamura, M.; Honda, M.; Nishiizumi, K.; Kohl, C. P.; Kocimski, S. M.; and Arnold, J. R.: 1974, "Cosmic ray produced Mn and Be Radionuclides in the Lunar Regolith." Proceedings of the Fifth Lunar Science Conference, Geochim. Cosmochim. Acta (in press).

Gold, T.: 1973, The Moon, Vol. 7, Nos. 3/4.

Harrington, T. M.; Marshall, J. H.; Arnold, J. R.; Peterson, L. E.; Trombka, J. I.; Metzger, A. E.: 1974, "The Apollo Gamma-Ray Spectrometer." Nuc. Instruments and Methods, (in press).

Hodges, C. A.: 1973, "Mare Ridges and Lava Lakes." Apollo 17 Preliminary Science Report, NASA SP-330, 31-12 - 31-21.

Kocharov, G. E.; and Victorov, S. V.: 1974, Doklady, Akad. Nauk USSR, in press.

Lingenfelter, R. E.; Canfield, E. H.; and Hampel, V. E.: 1972, "The Lunar Flux Revisited." Earth Planet. Sci. Letters, Vol. 16, 355.

Lowman, P.: 1972, "The Geologic Evolution of the Moon." J. of Geology, Vol. 80, No. 2, 125-166.

"Lunar Sample Preliminary Examination Team, " 1971, Science, 1 Vol. 173, 681.

Metzger, A. E.; Trombka, J. I.; Peterson, L. E.; Reedy, R. C.; and Arnold, J. R.: 1972, "A First Look at the Lunar Orbital Gamma-ray Data." Proceedings of the Third Lunar Science Conference, Geochim. Cosmochim. Acta, Suppl. 3, Vol. 3, frontispiece. MIT Press.

Metzger, A. E.: 1973, "Lunar Surface Radioactivity: Preliminary Results of the Apollo 15 and Apollo 16 Gamma-Ray Spectrometer Experiments," Science, 179, 800-803.

Metzger, A. E.; Trombka, J. I.; Peterson, L. E.; Reedy, R. C.; and Arnold, J. R.: 1974, "Element Concentration from Lunar Orbital Gamma-Ray Measurements." Proceedings of the Fifth Lunar Science Conference, Geochim. Cosmochim. Acta (in press).

Morris, E. C.; and Wilhelms, D. E.: 1967, Geologic Map of the Julius Caesar Quadrangle of the Moon; U. S. Geological Survey Map I-510.

O'Kelley, G. D.; Eldridge, J. S.; Schonfeld, E.; and Bell, P. R.: 1971, "Abundances of the Primordial Radionuclides K, Th, and U in Apollo-12 Lunar Samples by Non-destructive Gamma-ray Spectrometry; Implications for Origin of Lunar Soils," Proceedings of the Second Lunar Science Conference, Geochim. Cosmochim. Acta, Suppl 2, Vol. 2, 1159.

Patterson, James H.; Turkevitch, Anthony, L.; Franzgrote, E. J.; Economou, T. E.; and Sowinski, E. P.: 1972, Science, Vol. 168, 825.

Podwysocki, M. H.; Weidner, J. R.; Andre, C. G.; Beckel, A. L.; Lum, R. S.; Adler, I.; and Trombka, J. I.: 1974a, "An Analysis of the Apollo-15 X-ray Fluorescence Experiment for Detailed Lunar Morphological and Geochemical Parameters." Proceedings of the Fifth Lunar Science Conference, Geochim. Cosmochim. Acta (in press).

Podwysocki, M. H.; Andre, G. G.; Wiedner, J. R.: 1974b, "Quantitative Analysis of the Apollo X-Ray Fluorescent Analysis for the Extraction of Detailed Geologic Information." NASA X-Document (in preparation).

Proceedings of the Fourth Lunar Science Conference, Geochim. Cosmochim. Acta, Suppl. 4, Vol. 1, Frontispiece 1973, plate II.

Reedy, R. C. and Arnold, J. R.: 1972, "Interaction of Solar and Galactic Cosmic Ray Particles with the Moon." J. Geophys. Res., Vol. 77, 537.

Reedy, R. C.; Arnold, J. R.; and Trombka, J. I.: 1973, "Expected Gamma-ray Emission Spectra from the Lunar Surface as a Function of Chemical Composition." J. Geophys. Res., Vol. 78, 5847-5866.

Schonfeld, E.; and Meyer, C.: 1972, "The Abundances of Components of the Lunar Soils by a Least Squares Mixing Model and the Formation Age of KREEP." Proceedings of the Third Lunar Science Conference, Geochim. Cosmochim. Acta, Suppl. 3, Vol. 2, 1397-1420.

Scott, P. H.; and Pohn, H. A.: 1972, Geologic Map of the Macrobius Quadrangle of the Moon; U. S. Geological Survey Map I-799.

Sjogren, W. L.; and Wollenhaupt, W. R.: 1973, "Lunar Shape via the Apollo Laser Altimeter." Science, Vol. 179, 275-278.

Trombka, J. I.; Arnold, J. R.; Reedy, R. C.; Peterson, L. E.; and Metzger, A. E.: 1973, "Some Correlations Between Measurements by the Apollo Gamma-ray Spectrometer and Other Lunar Observations." 1973 Proceedings of the Fourth Lunar Science Conference, Geochim. Cosmochim. Acta, Suppl. 4, Vol. 3, 2847-2853.

Turkevich, A. L.; Franzgrote, E. J.; and Patterson, J. H.: 1969, "Chemical Composition of the Lunar Surface in Mare Tranquillitatis." Science, Vol. 165, 277.

Wakita, H.; Schmitt, R. A.; and Rey, P.: 1970, "Elemental Abundances of Major, Minor and Trace Elements in Apollo 11 Lunar Rocks." Apollo-11 First Lunar Science Conference, Geochim. Cosmochim. Acta, Suppl. 1, Vol. 2, 1685.

Whitaker, E. A.: 1965, The Nature of the Lunar Surface, The Surface of the Moon. Hess, Menzel and O'Keefe (eds.) The Johns Hopkins Press, 79.

Wilhelms, D. E.: 1972, Geologic Map of the Taruntius Quadrangle of the Moon; U. S. Geological Survey Map I-722.

Woolum, D. S.; and Burnett, D. S.: 1974, "In-situ Measurement of the rate of ^{235}U Fission Induced by Lunar Neutrons." Earth Planet. Sci. Letters, Vol. 21, 153.

Young, R. A.; Brennan, W. J.; Wolfe, R. W.; and Nichols, D. J.: 1973, "Volcanism in the Lunar Maria," Apollo-17 Preliminary Science Report, NASA SP-330, 31-1 - 31-11.

FIGURE CAPTIONS

- Figure 1. Pulse height spectrum obtained with a 7 cm by 7 cm NaI(Tl) detector, on a boom 7.6 m from the Apollo spacecraft. The measurement was made during the transearth phase of the Apollo-15 mission. Scale is ~ 19 keV/channel.
- Figure 2. Lowest and highest background used in the analysis of the Apollo-15 lunar spectrum. Crystal detector is 7 cm by 7 cm and at a boom position 7.6 m from the spacecraft. Scale is ~ 19 keV/channel.
- Figure 3. Pulse height spectrum corresponding to an average lunar spectrum for the Apollo-15 orbital mission. The derived average lunar background is also indicated. The pulse height spectra were obtained with the Apollo-15 gamma-ray spectrometer. Scale is ~ 19 keV/channel.
- Figure 4. Difference pulse height spectrums or discrete line lunar emission pulse height spectrum obtained with the Apollo-15 gamma-ray spectrometer over the whole ground track. The elemental components for O, Fe, Ti, Co, Th + U, Al, Si, Mg, and K are also indicated. The components were used for the least square analysis of the difference curve. The synthesized curve obtained from least square analysis is also shown. Scale is ~ 19 keV/channel.
- Figure 5. Pulse height spectra obtained with the Apollo-15 X-ray spectrometer. The spectrum was taken over Mare Crisium. Spectra shown are from the base detector (5a), the detector with the Mg filter (5b), and the detector with the Al filter (5c). The scale as shown has a lower level of 0.75 keV and is about 0.33 keV/channel. The data have been normalized so that the area under the base detector peak is unity.
- Figure 6. Distribution of lunar radioactivity in the energy region 0.55-2.75 MeV over the Apollo-15 and Apollo-16 ground tracks. The data are presented on a 5- by 5-degree scale over a base map freely adopted from one furnished by Dr. Farouk El Baz.

- Figure 7. Profile of lunar topography and natural radioactivity across the Apollo-15 and Apollo-16 ground tracks as measured by the laser altimeter and gamma-ray spectrometer. The deviation is represented by the line, radioactivity plus the underlying continuum by the points.
- Figure 8. The region around the crater Van de Graaff, showing the altitude-corrected, gamma-ray intensities between 0.55 MeV and 2.75 MeV in 2- by 2-degree areas, the location of the laser altimeter ground track with elevation given at the top, and a contour map of the lunar contribution to the solar-directed component of the magnetic field from an elevation of 67 km. The subsatellite magnetometer values are in tenths of gammas. The insert gives the coding which represents the observation time within the 2- by 2-degree area, and the maximum 1σ standard deviation corresponding to that period.
- Figure 9. Areas on the moon used in the lunar data analysis (see Table 2 for key).
- Figure 10. (a) Potassium and thorium on the lunar surface, plotted against longitude on the Apollo-15 ground track.
(b) The same plot for Apollo-16.
- Figure 11. (a) Al/Si ratio versus longitude for the Apollo-15 ground northern track. The values for some reference material are shown.
(b) Mg/Si ratios for the same tracks as above northerly track.
- Figure 12. (a) Al/Si for the Apollo-15 southern ground track.
(b) Mg/Si for the same southern track.
- Figure 13. (a) Al/Si for the Apollo-16 ground track.
(b) Mg/Si for the same track.
- Figure 14. A comparison of Al/Si intensity ratios versus optional albedo values for various Apollo-16 orbits.
- Figure 15. Fourth order trend surface map for Al/Si intensity ratios using 16-second data. (Podwysocki, 1974a).

Figure 16. Residuals from the fourth order trend surface for Al/Si intensity ratios. Departures or deviations are based on normalized data. A plus sign denotes a positive residual; a negative sign indicates a negative residual. Calculated intensity ratios are given in original units for ease of interpretation (Podwysocki, 1974a).

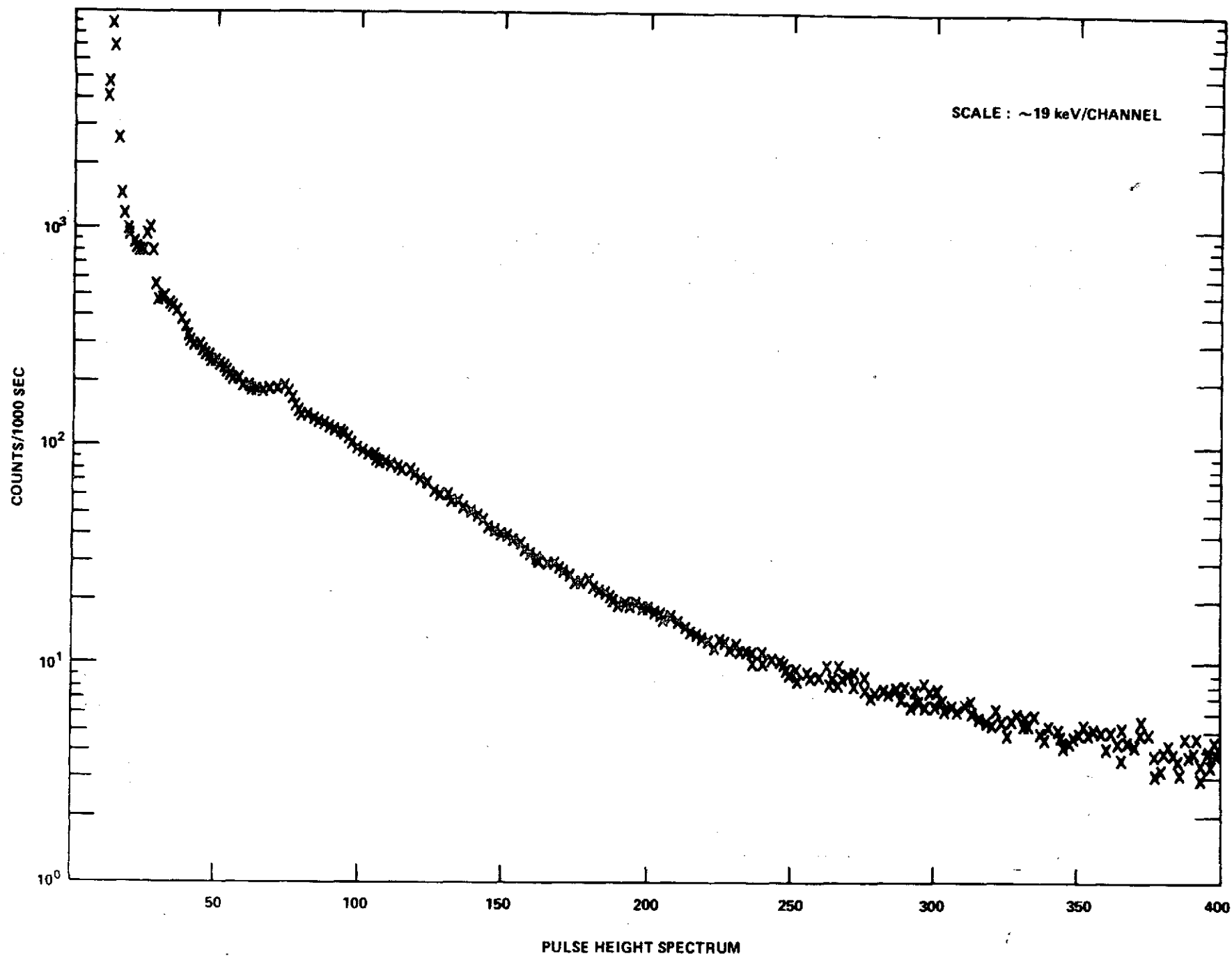


Figure 1.

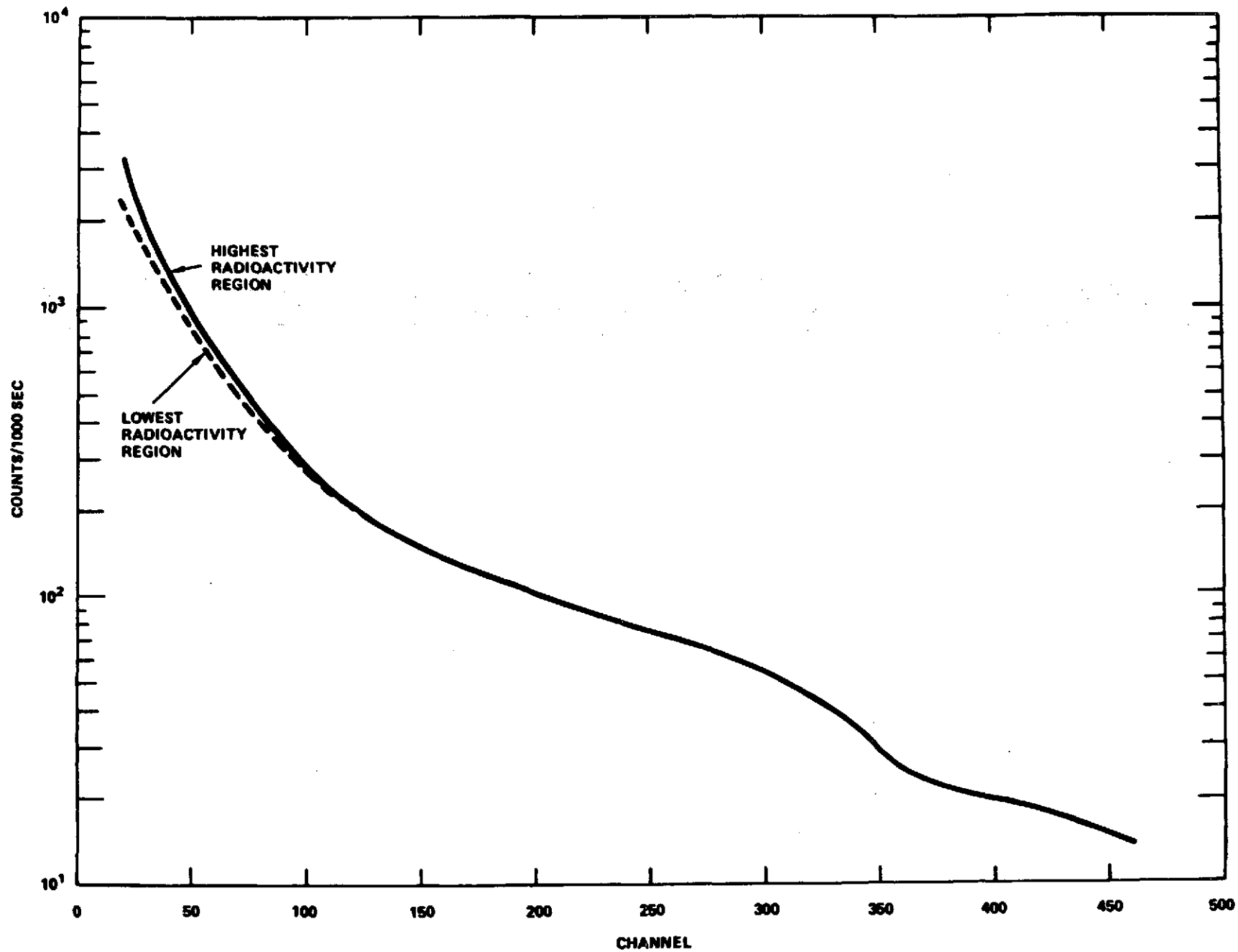


Figure 2.

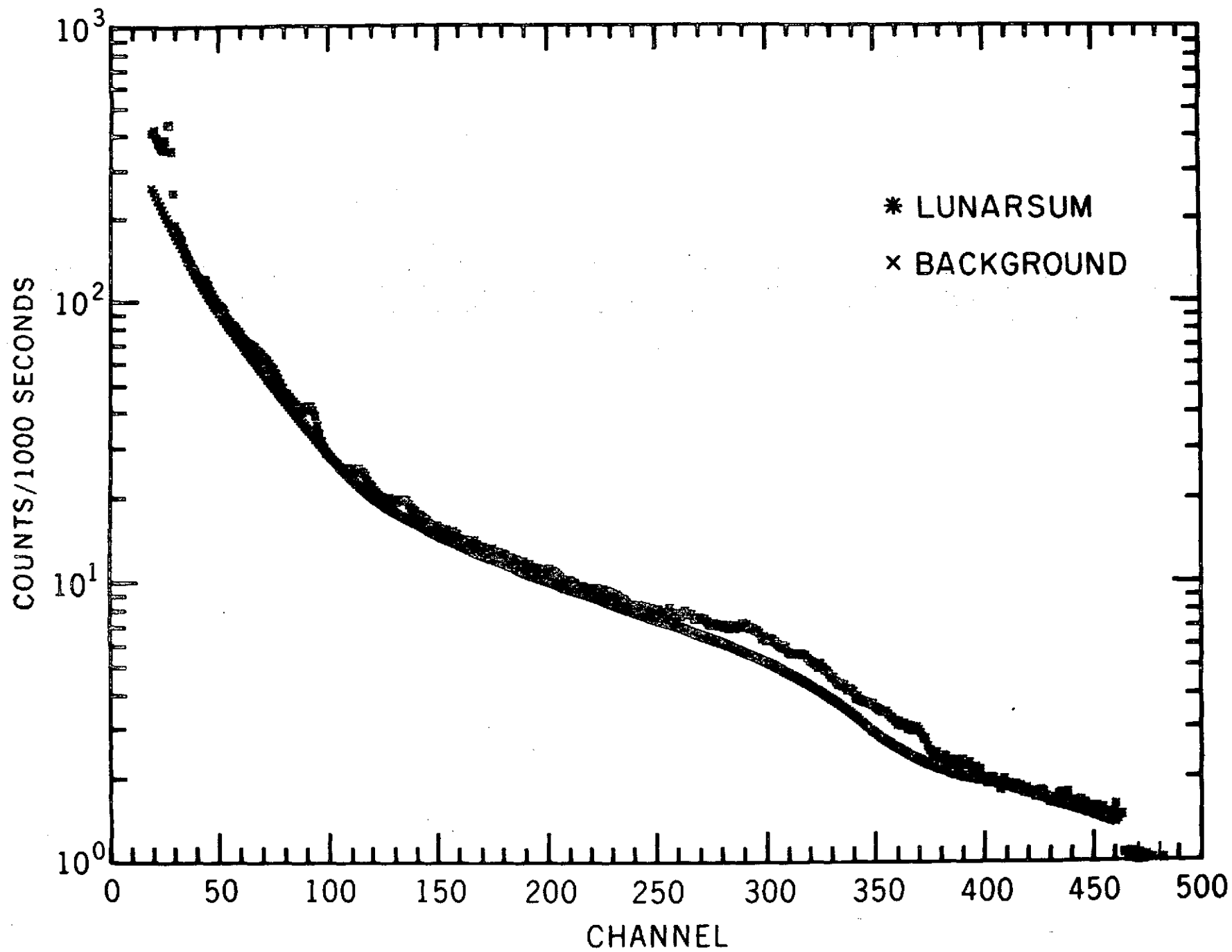


Figure 3.

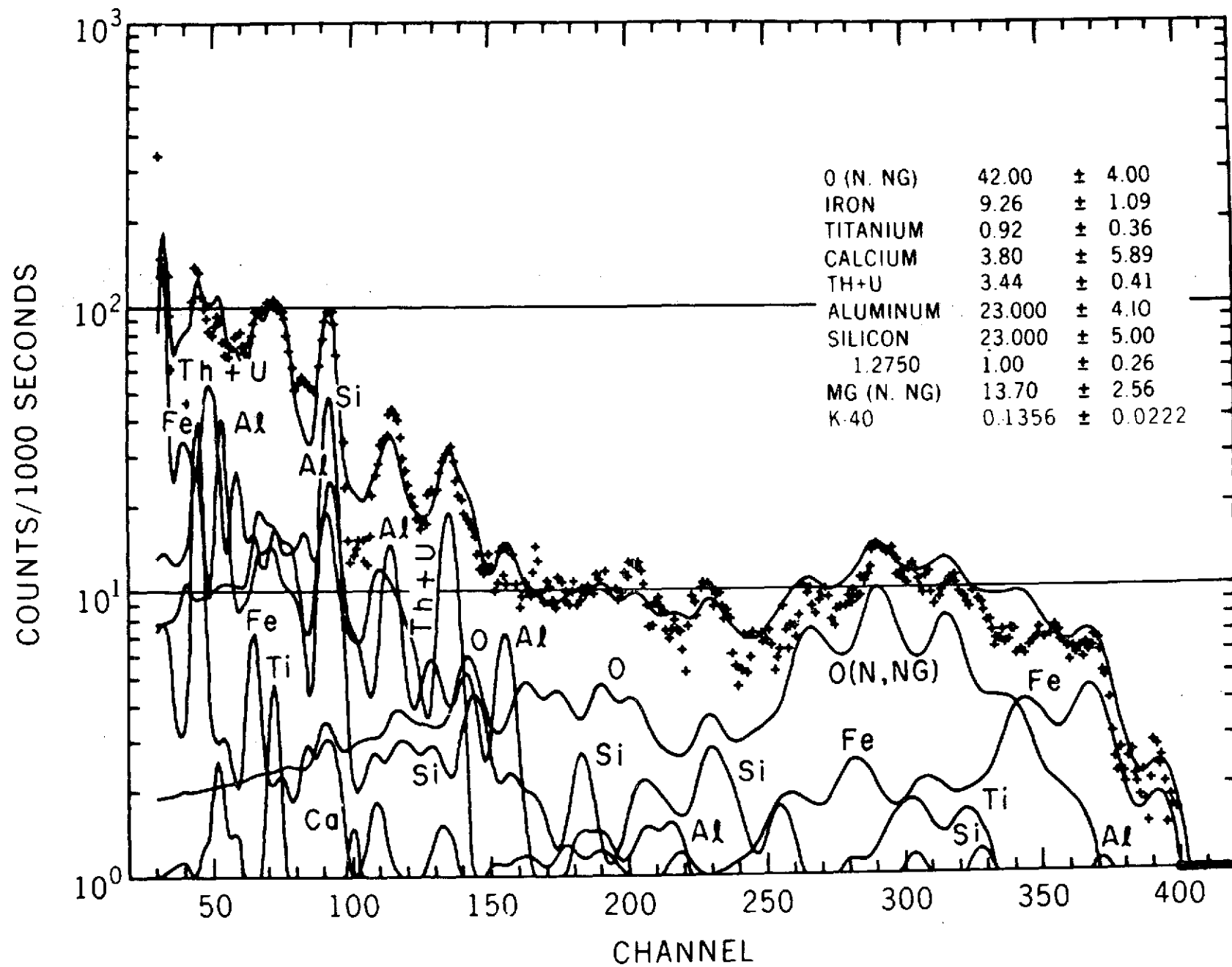
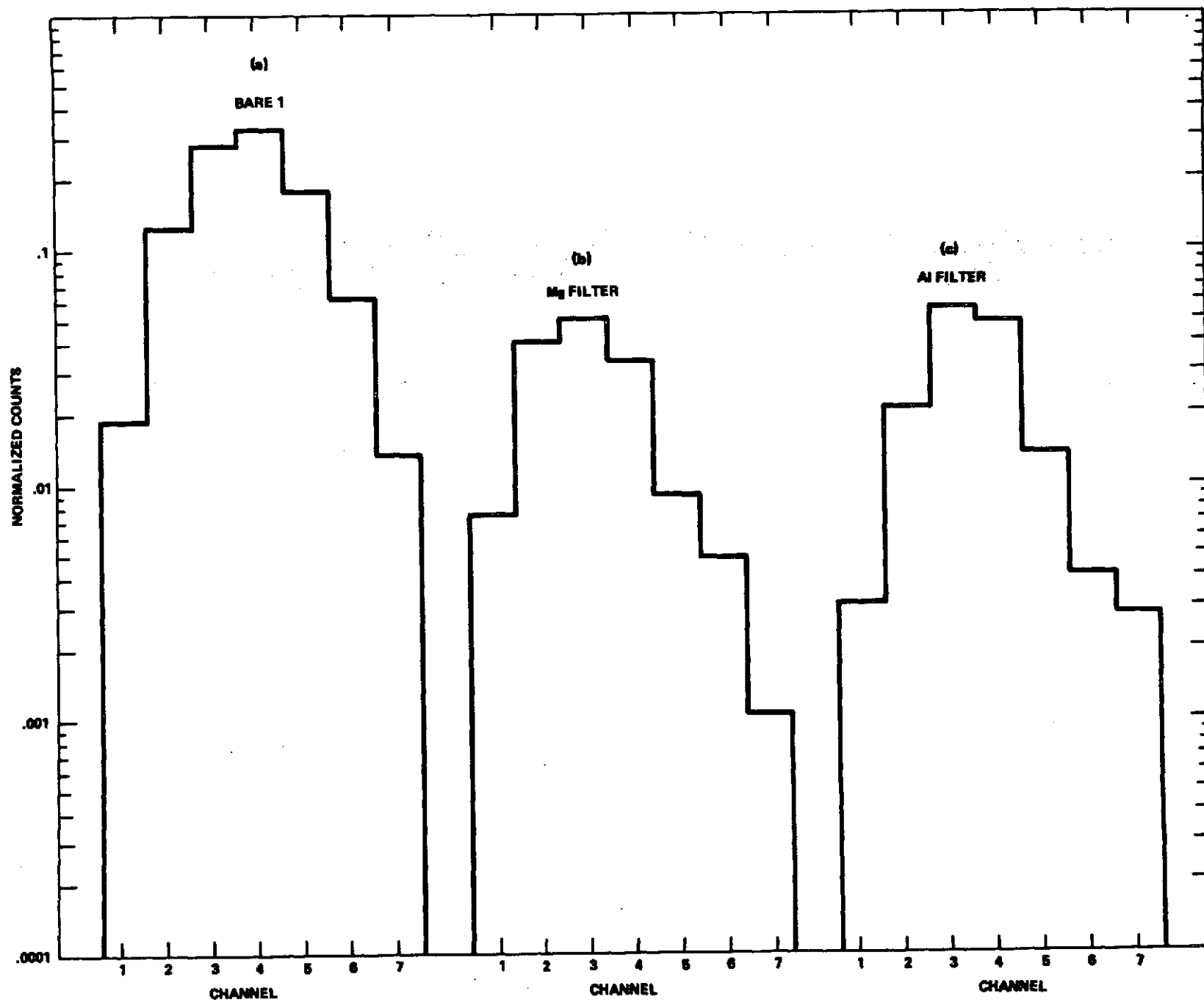


Figure 4.



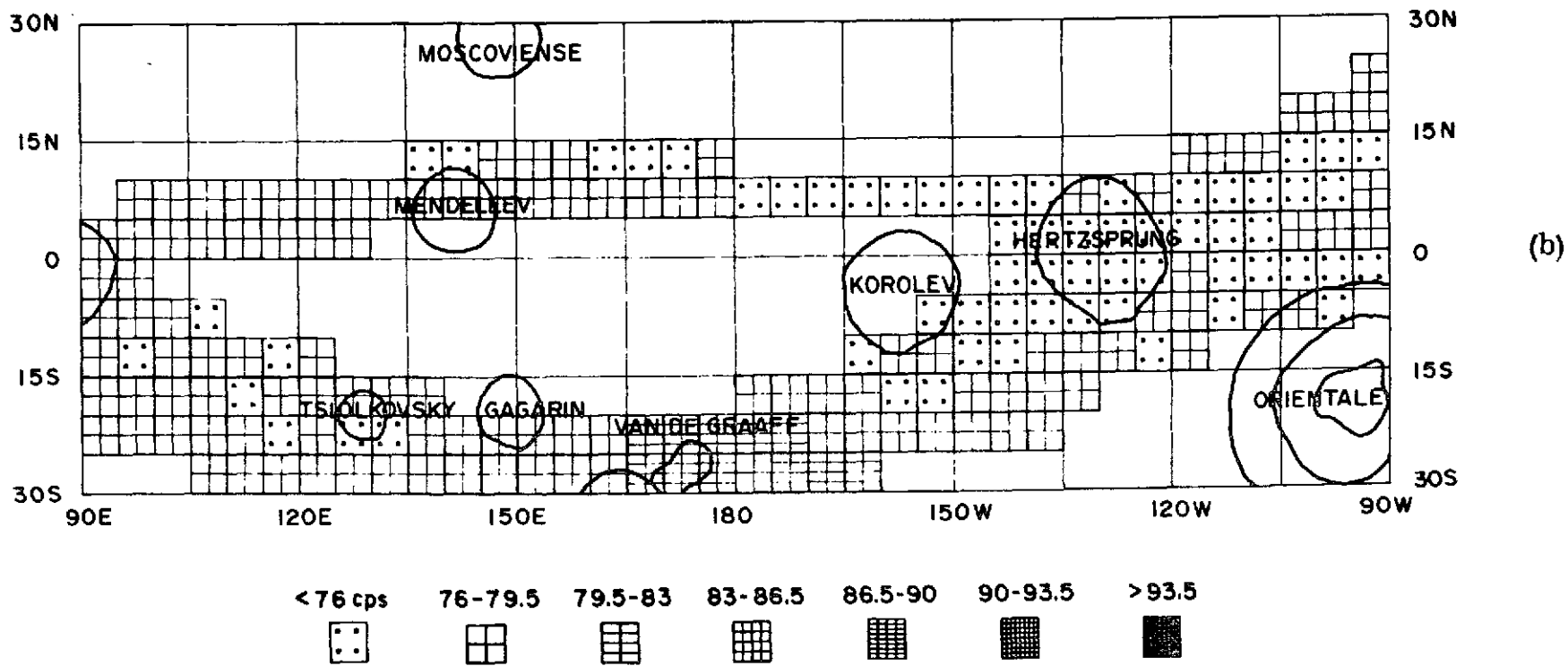
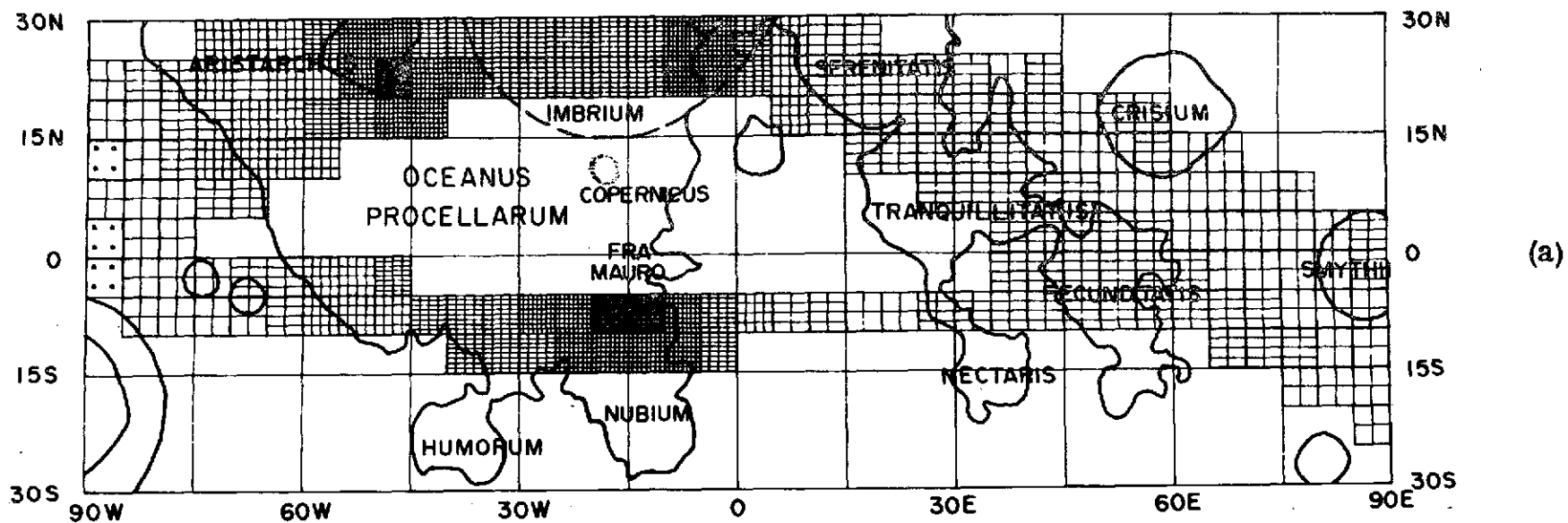


Figure 6

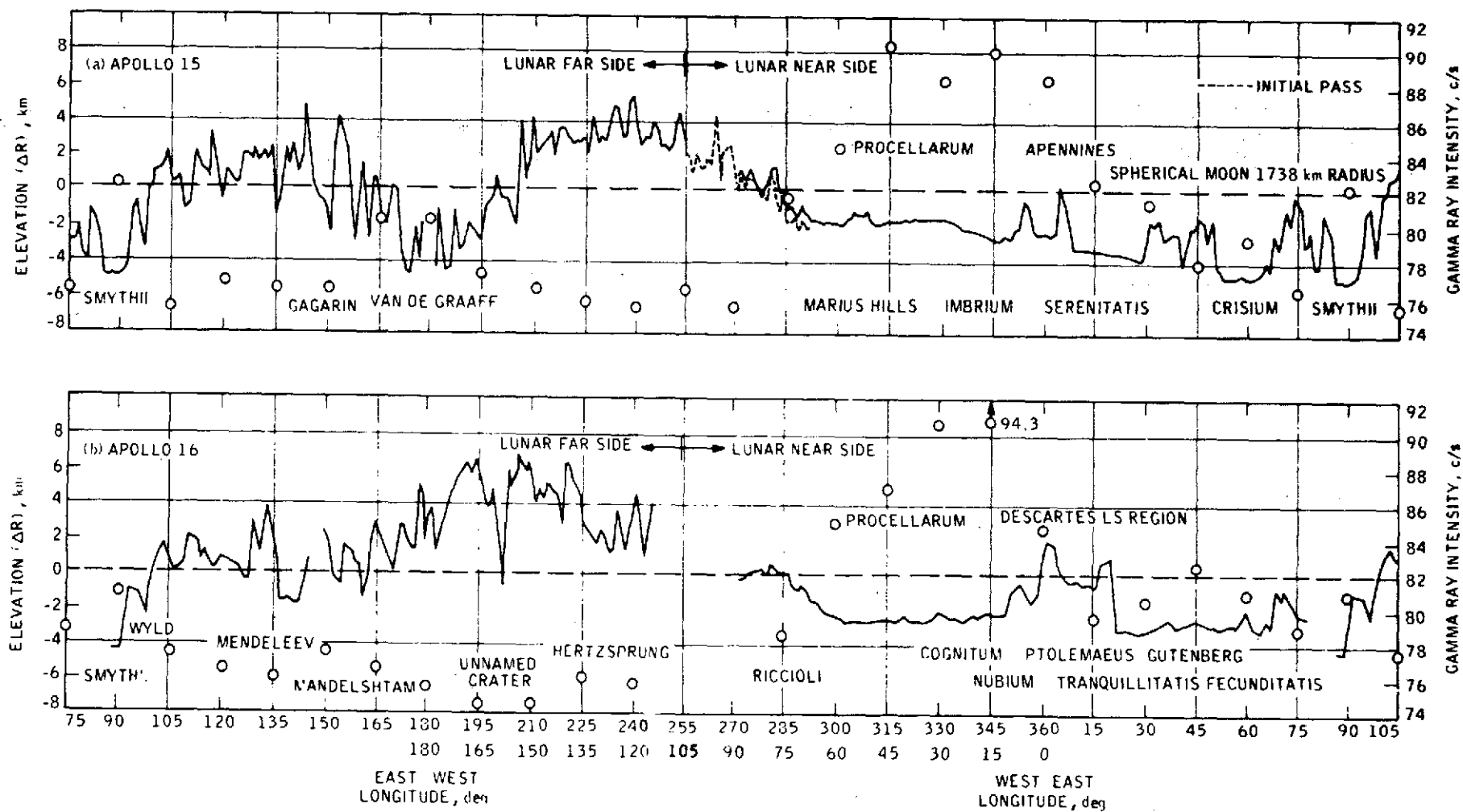


Figure 7.

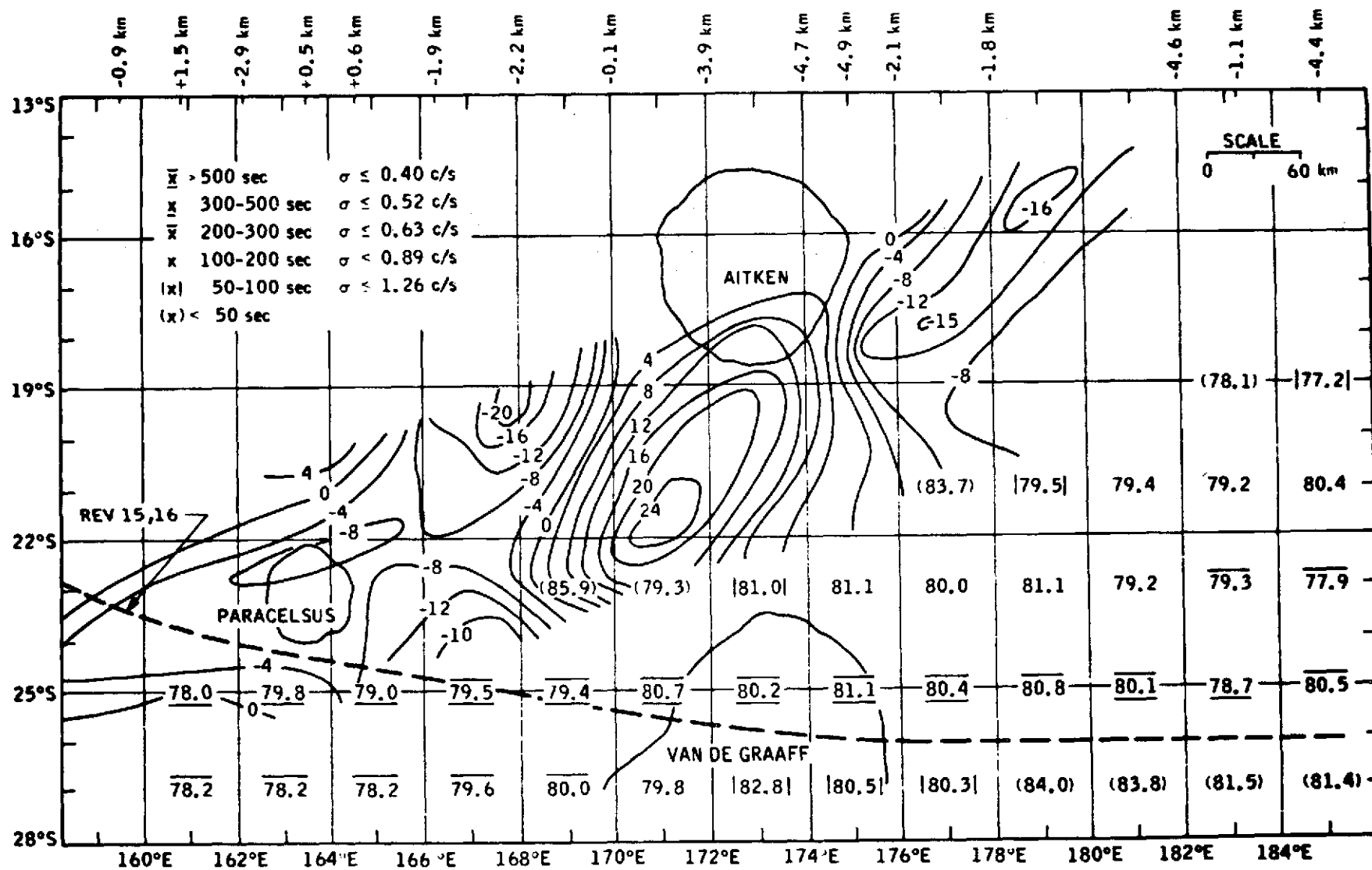
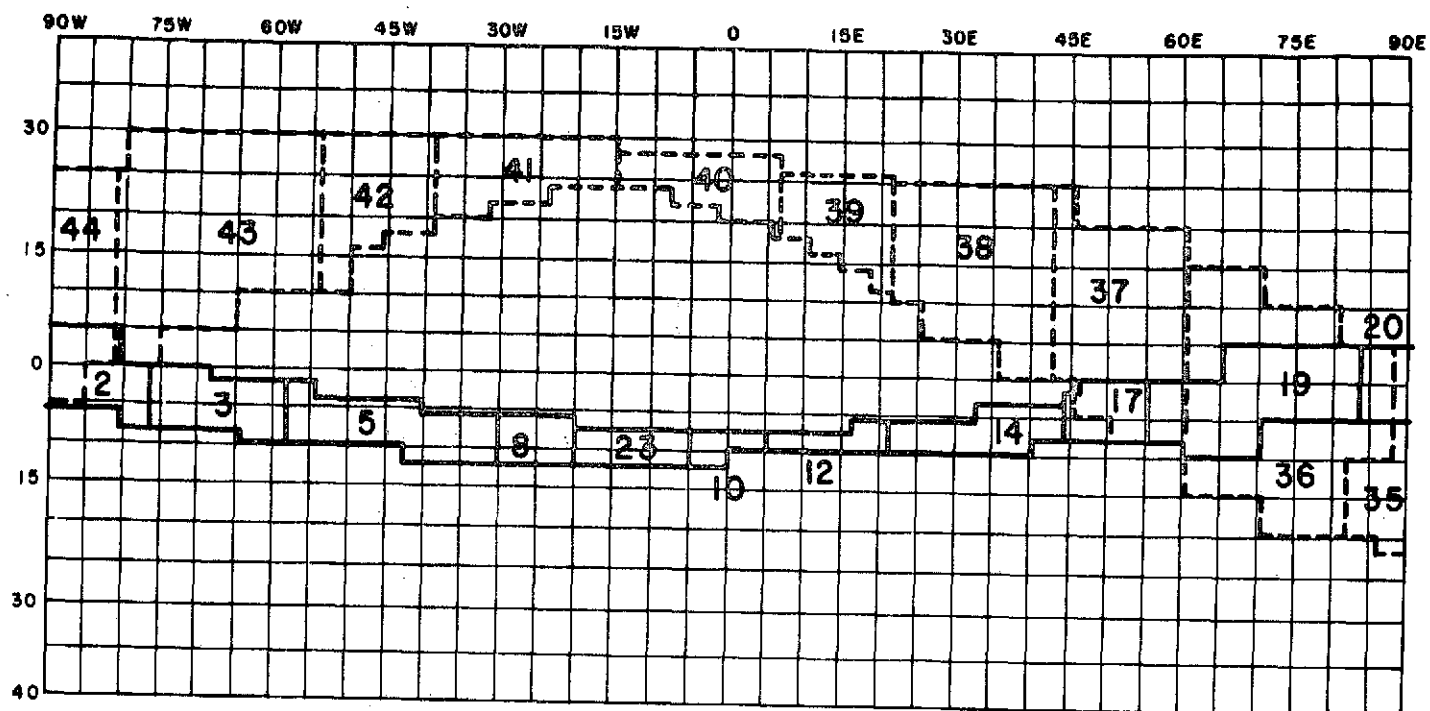
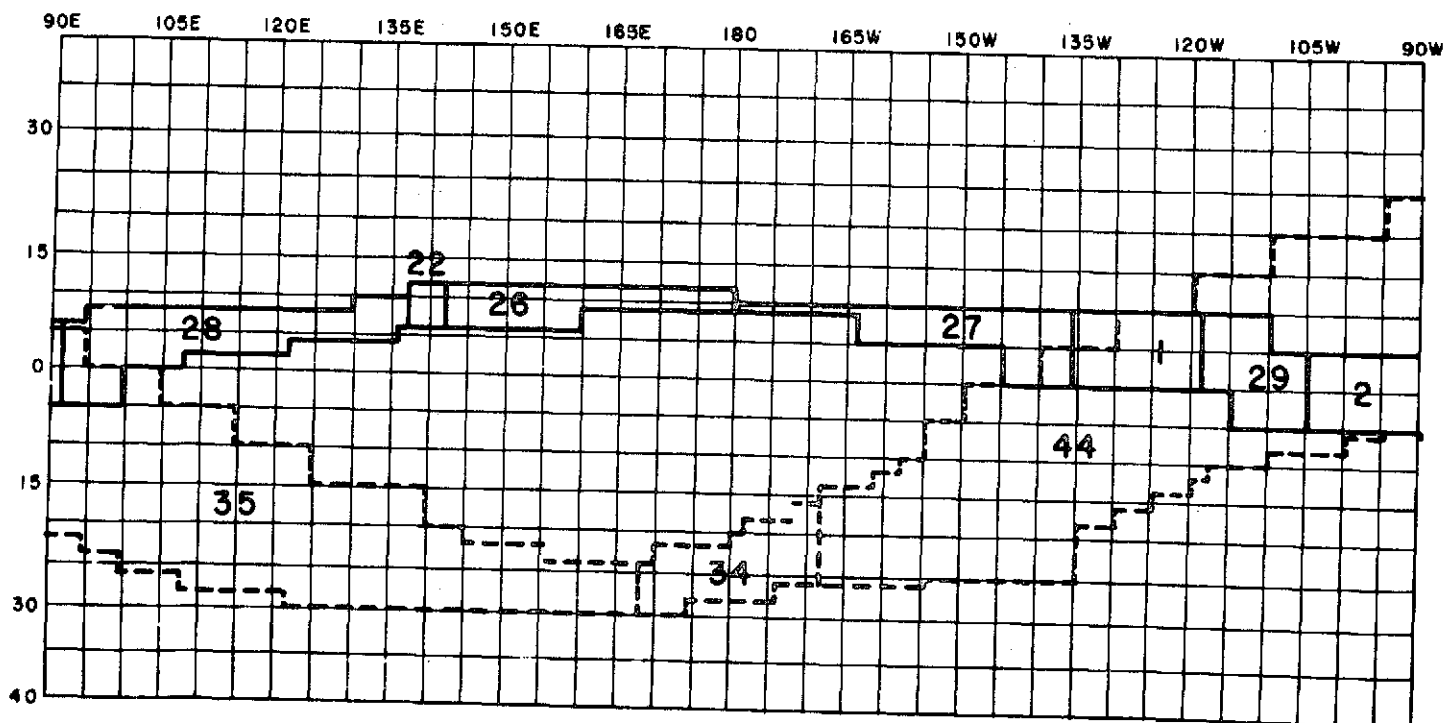


Figure 8.



LUNAR NEARSIDE



LUNAR FAR SIDE

Figure 9.

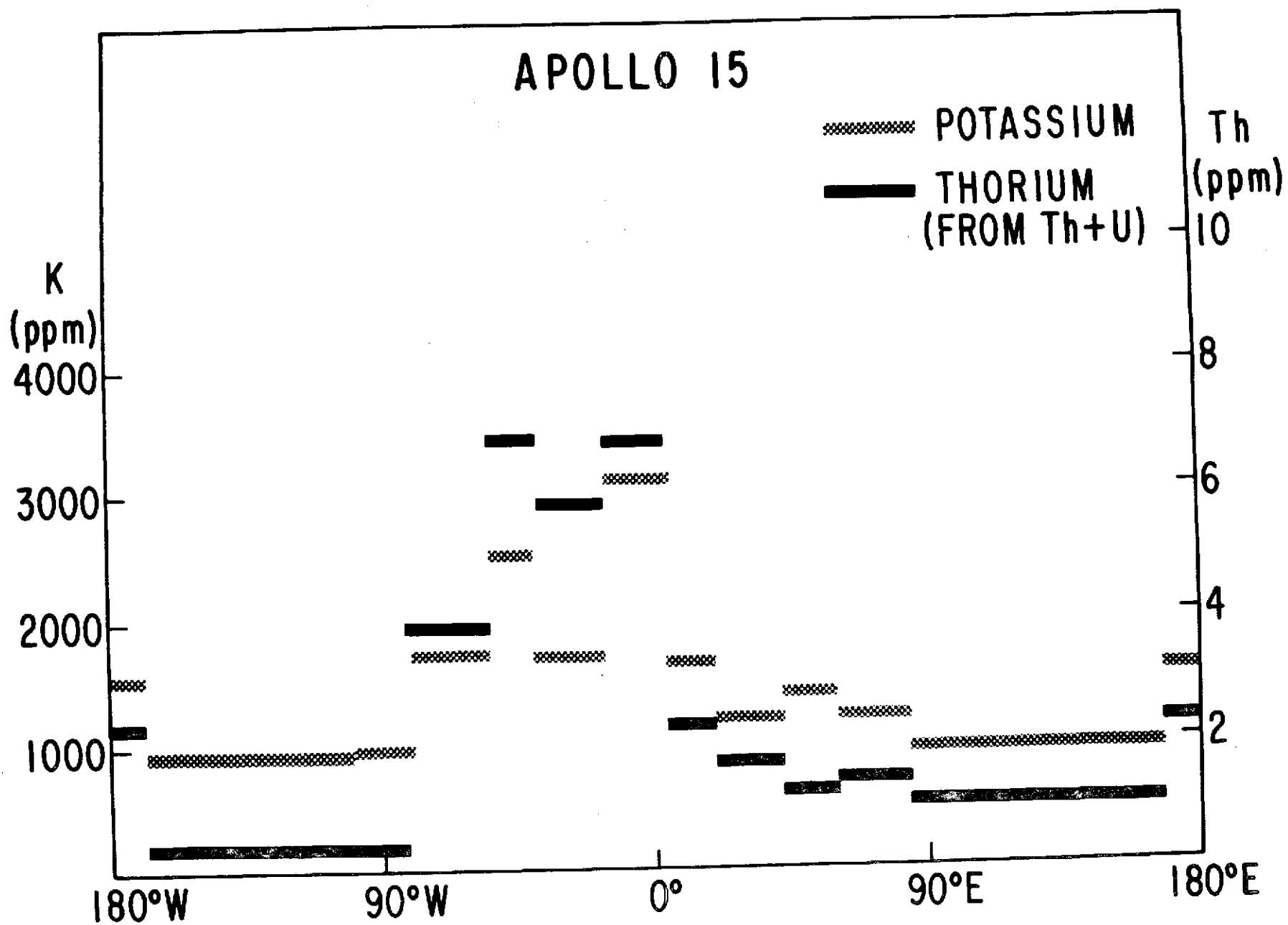


Figure 10a.

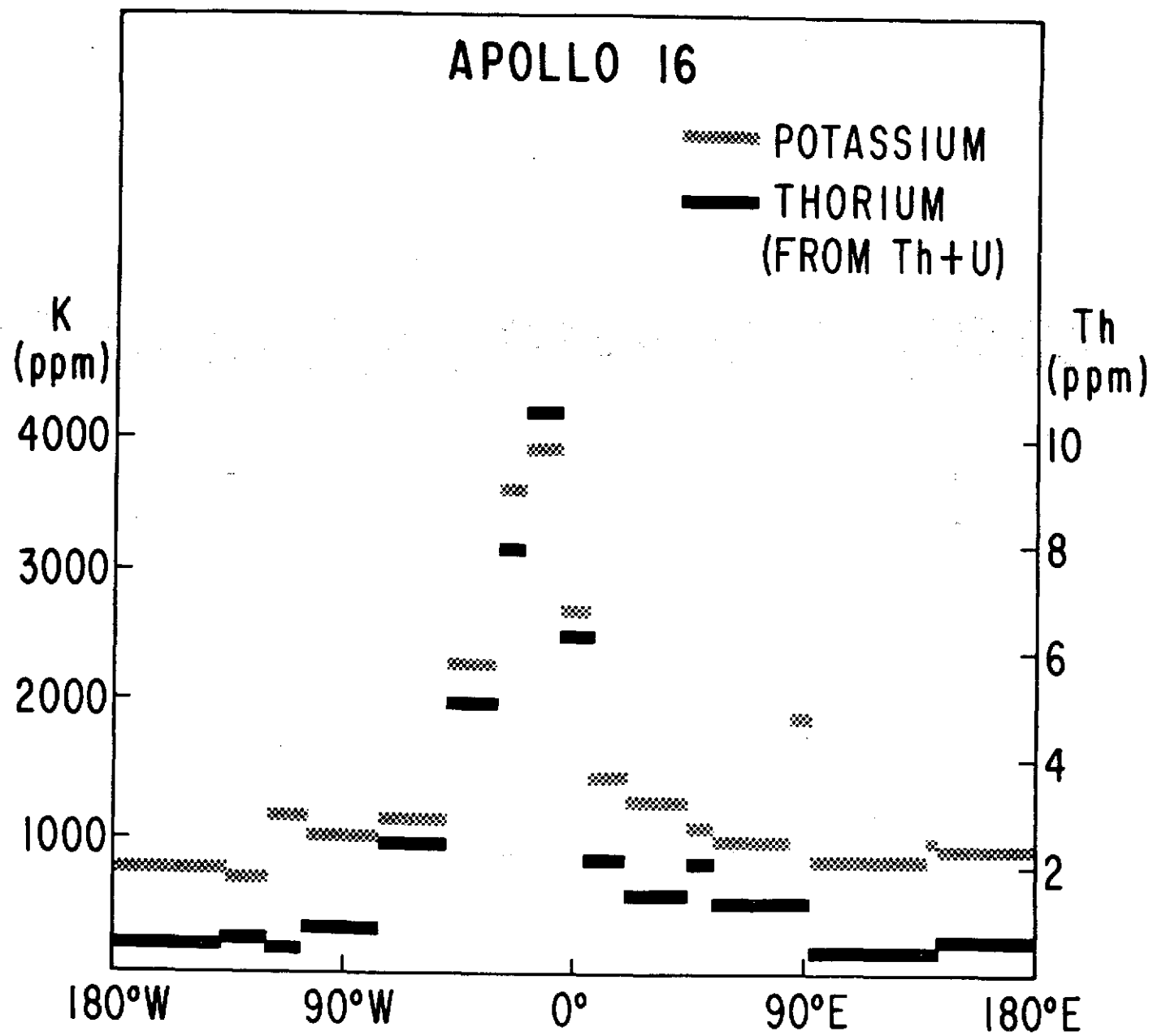


Figure 10b.

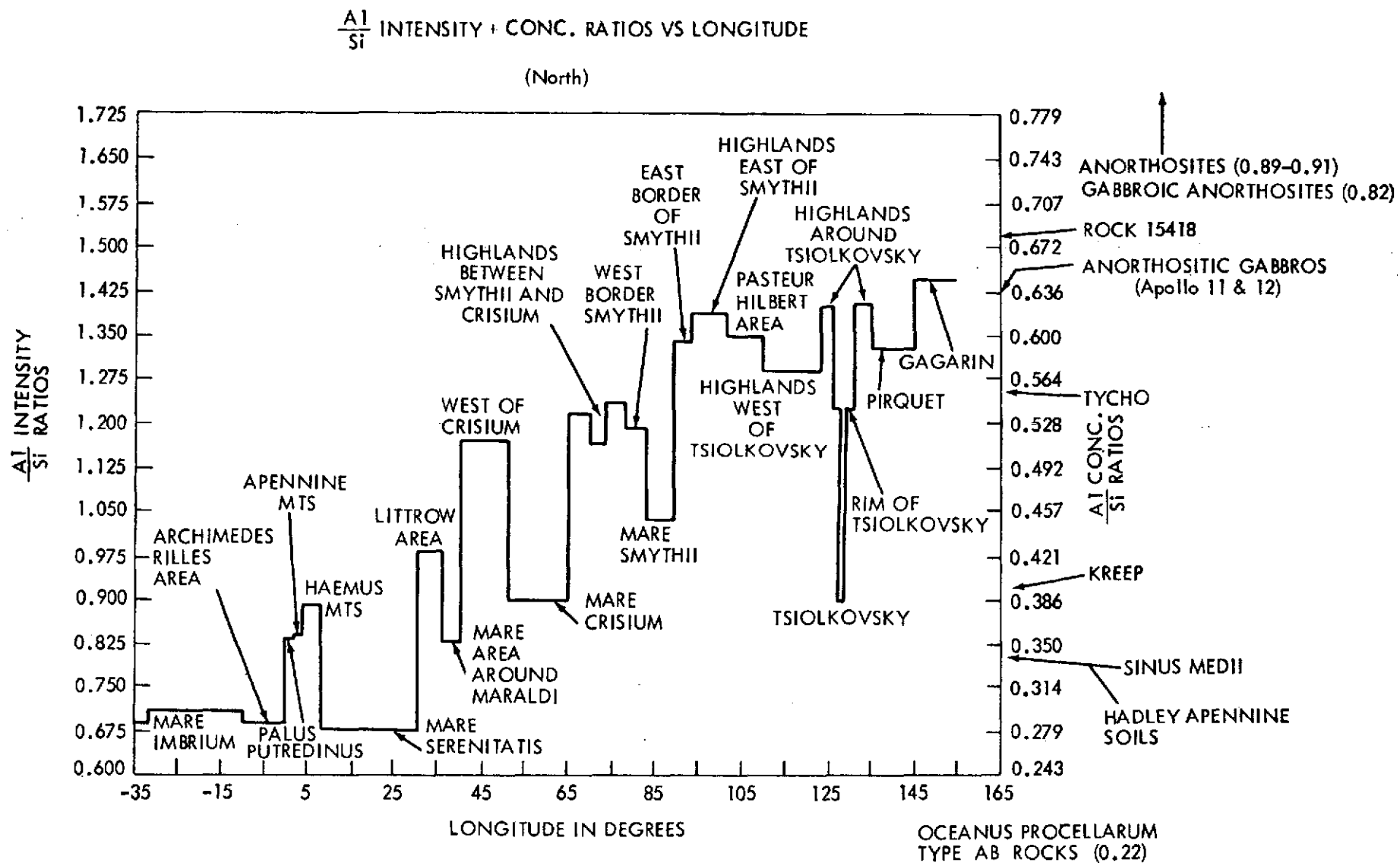


Figure 11a.

$\frac{Mg}{Si}$ INTENSITY & CONC. RATIOS VS LONGITUDE

(North)

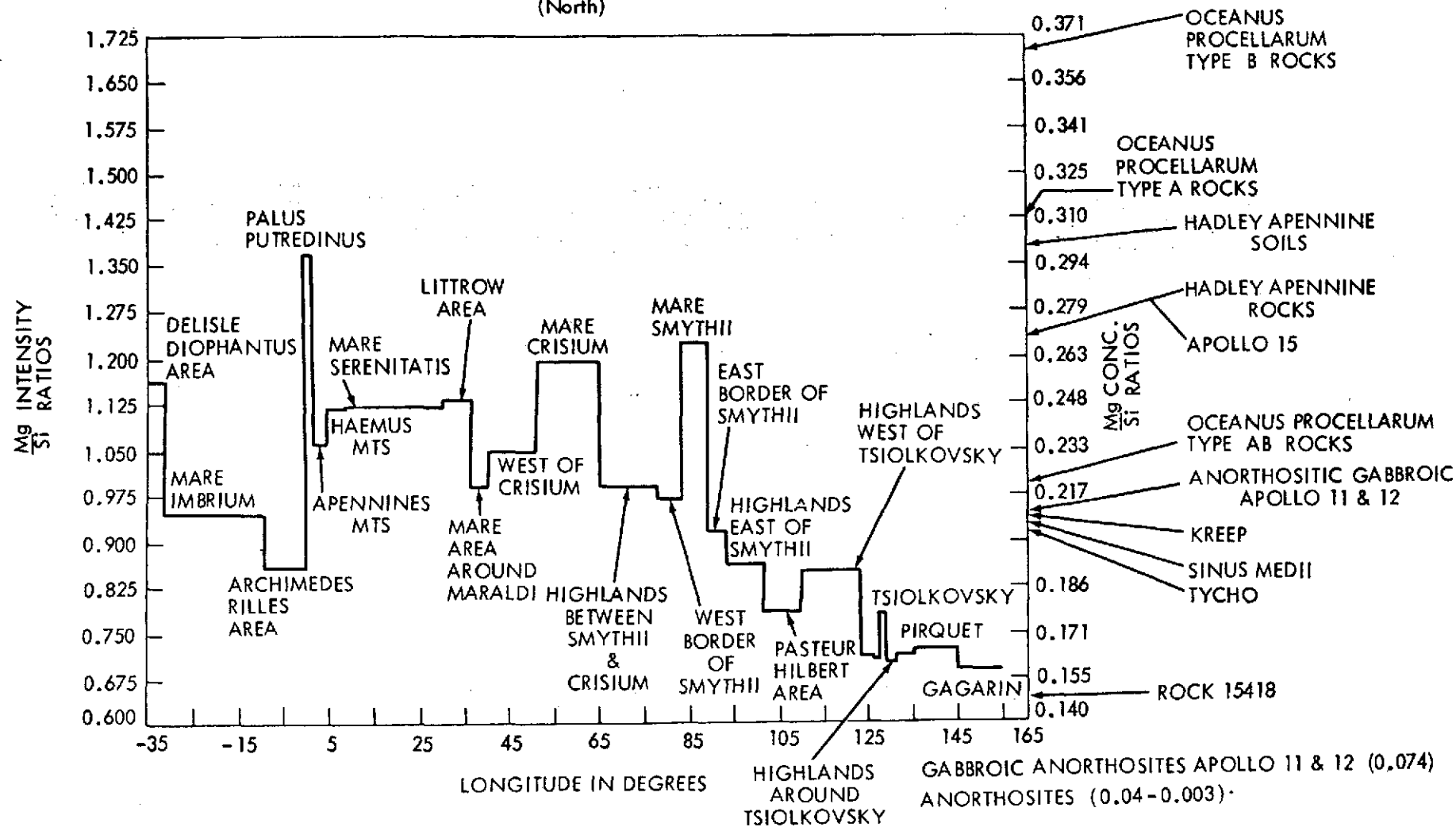


Figure 11b.

$\frac{Al}{Si}$ INTENSITY & CONC. RATIOS VS LONGITUDE
(South)

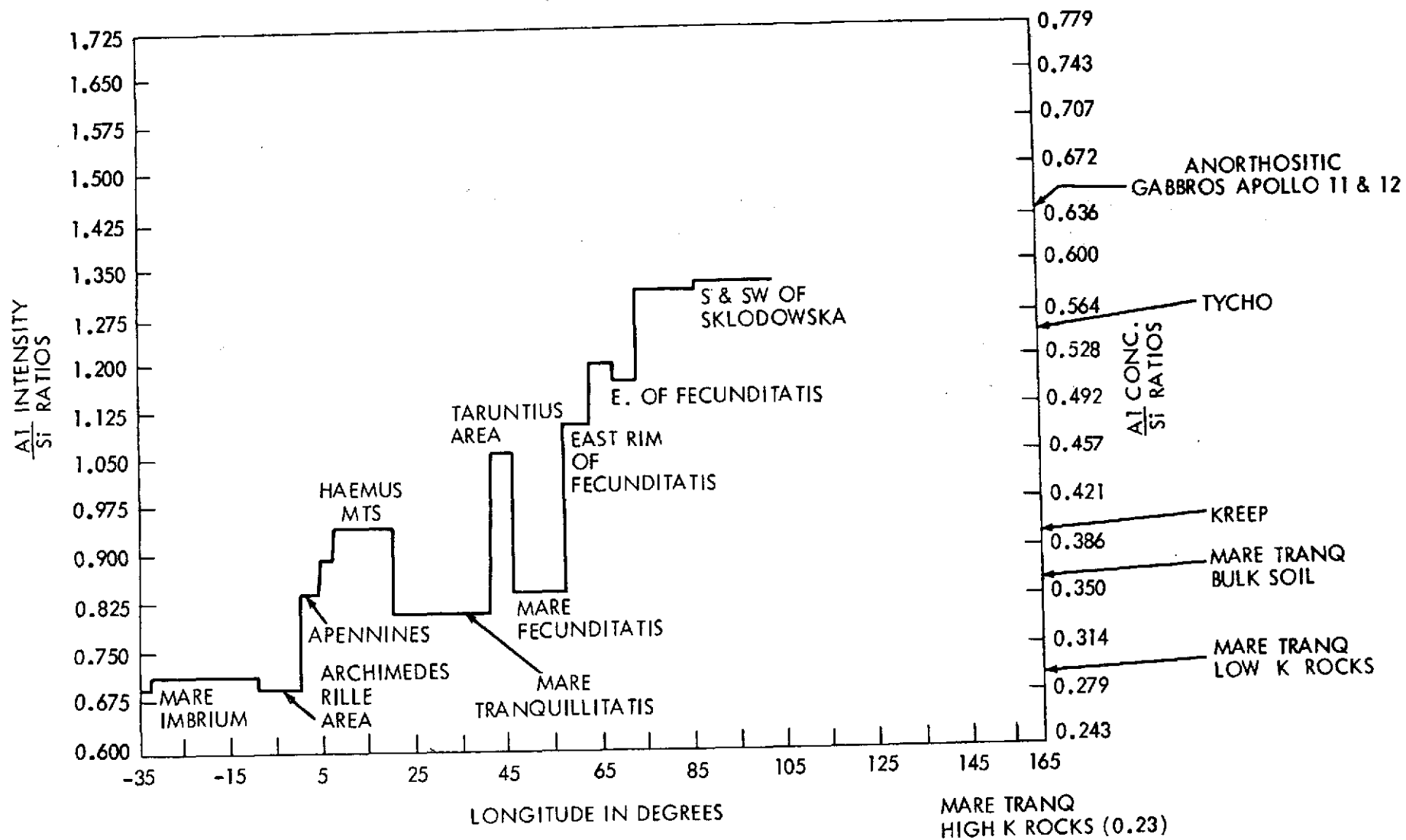


Figure 12a.

$\frac{\text{Mg}}{\text{Si}}$ INTENSITY & CONC. RATIOS VS LONGITUDE

(South)

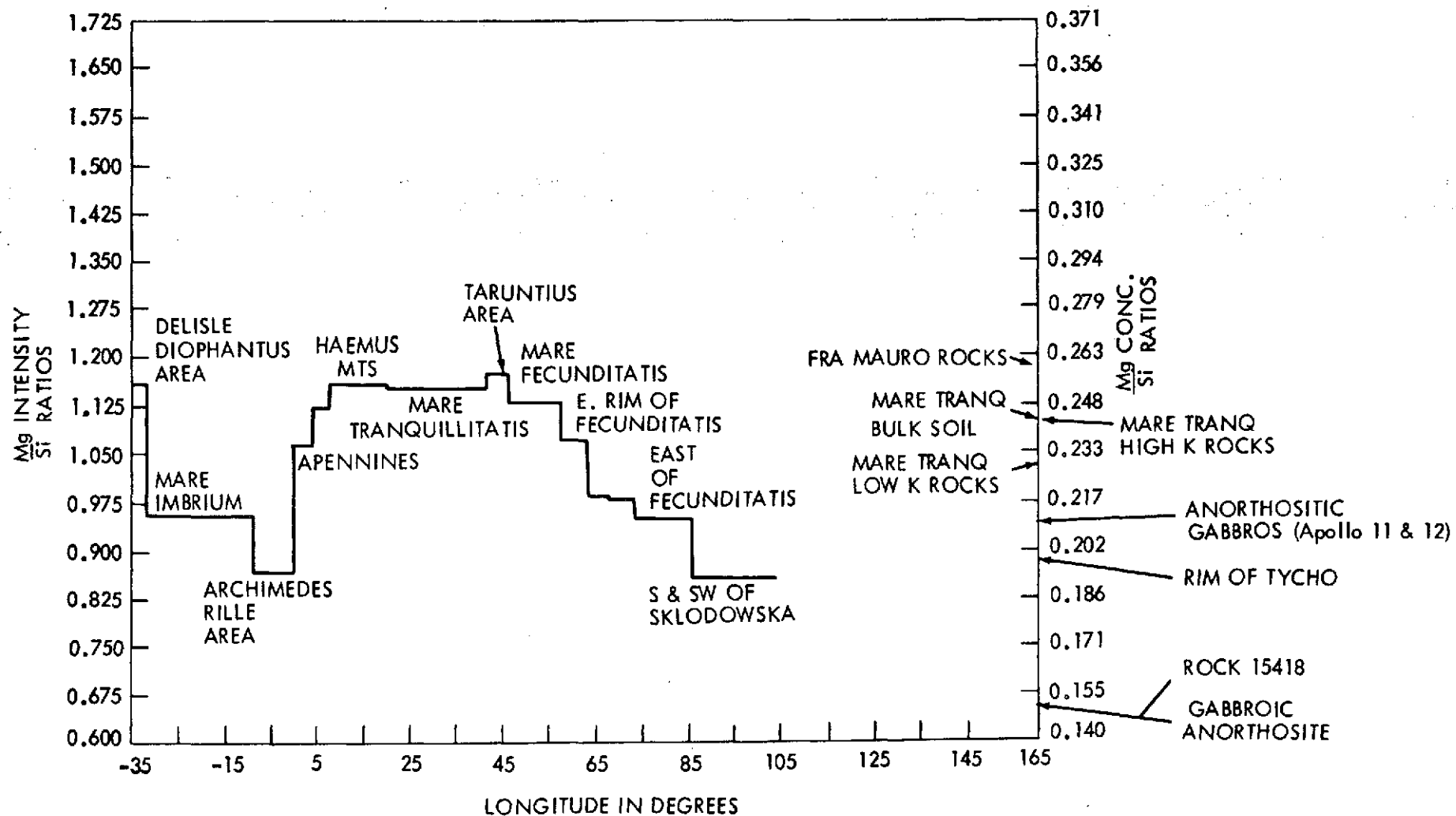


Figure 12b.

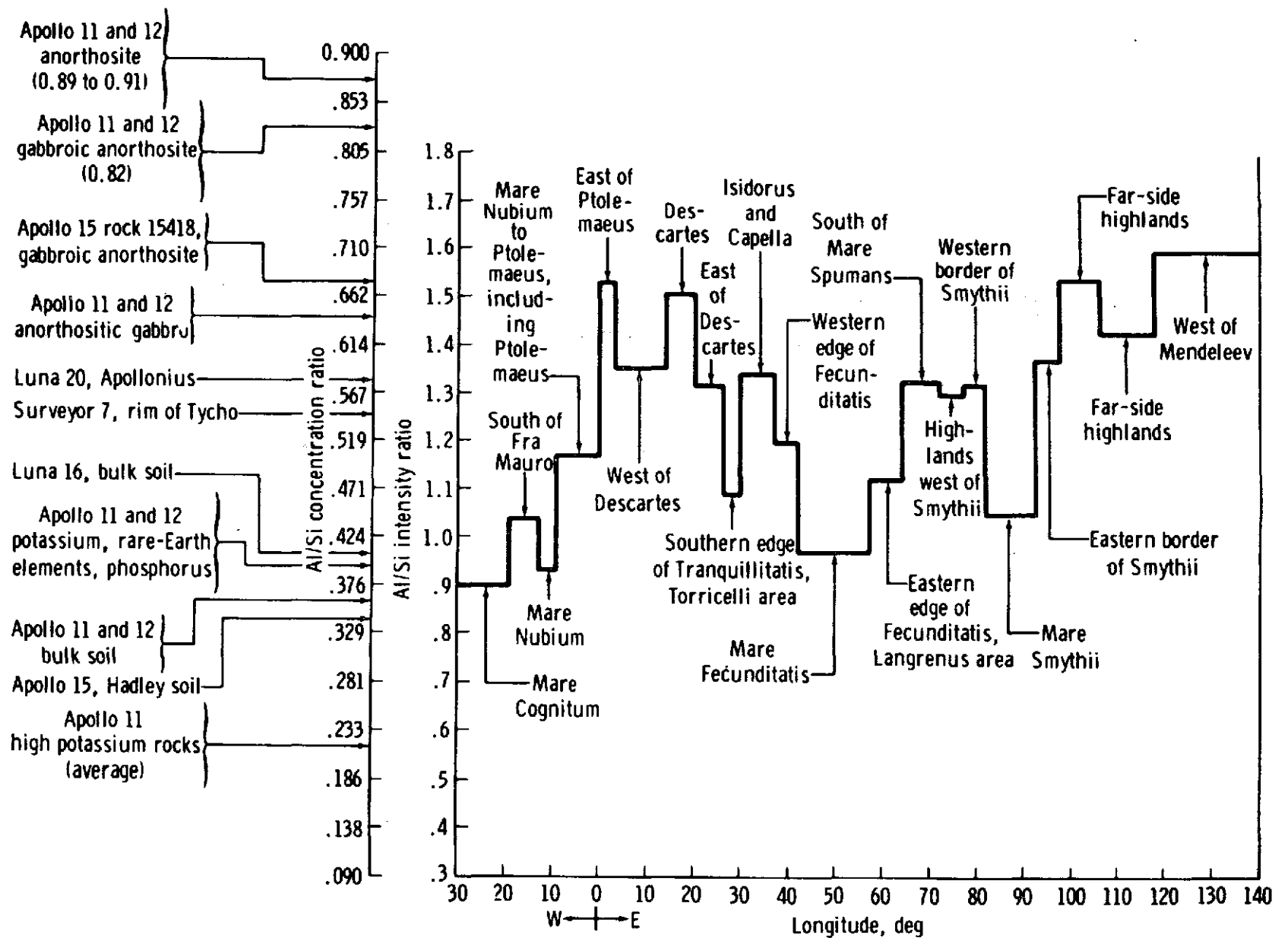


Figure 13a.

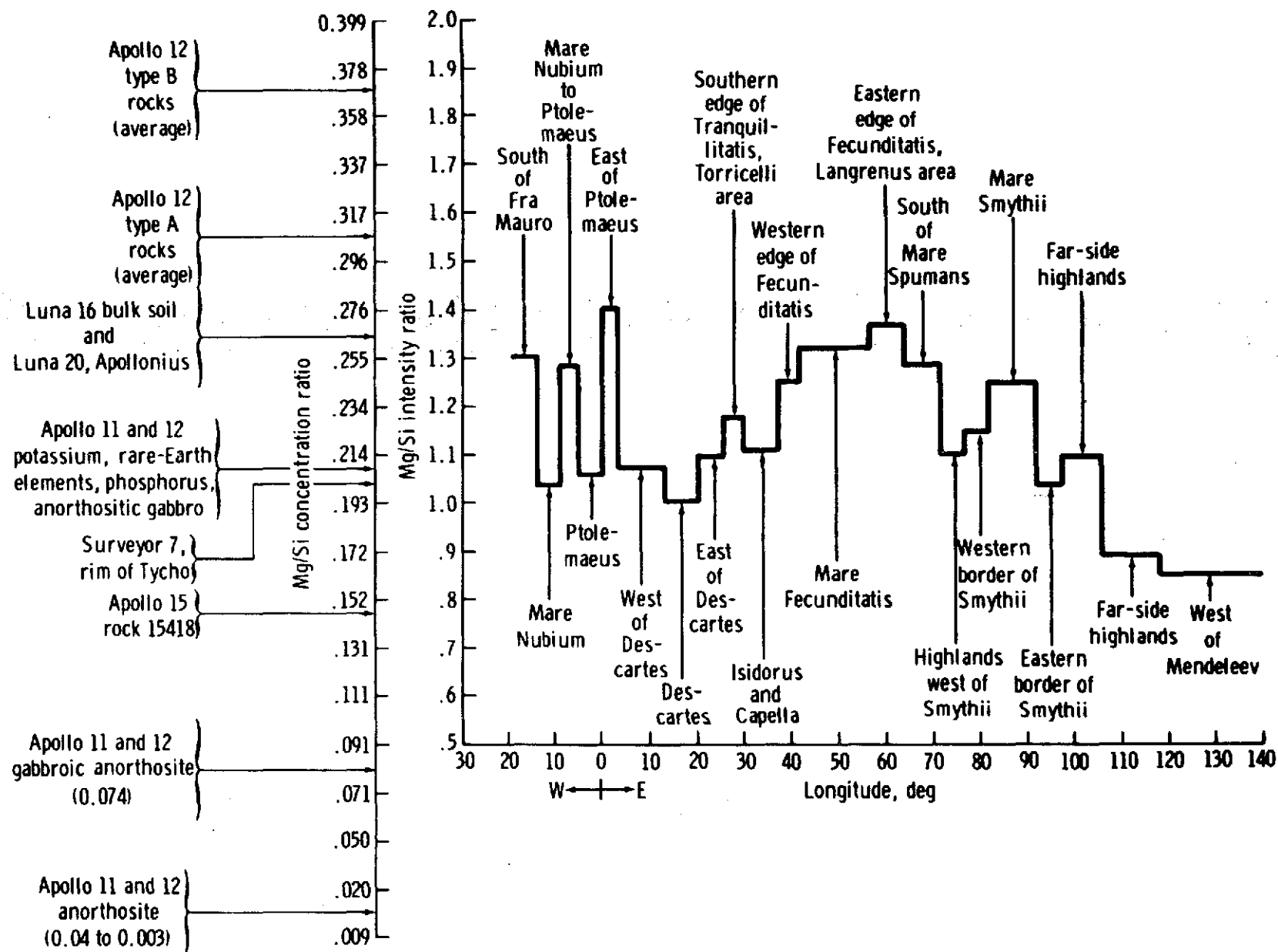


Figure 13b.

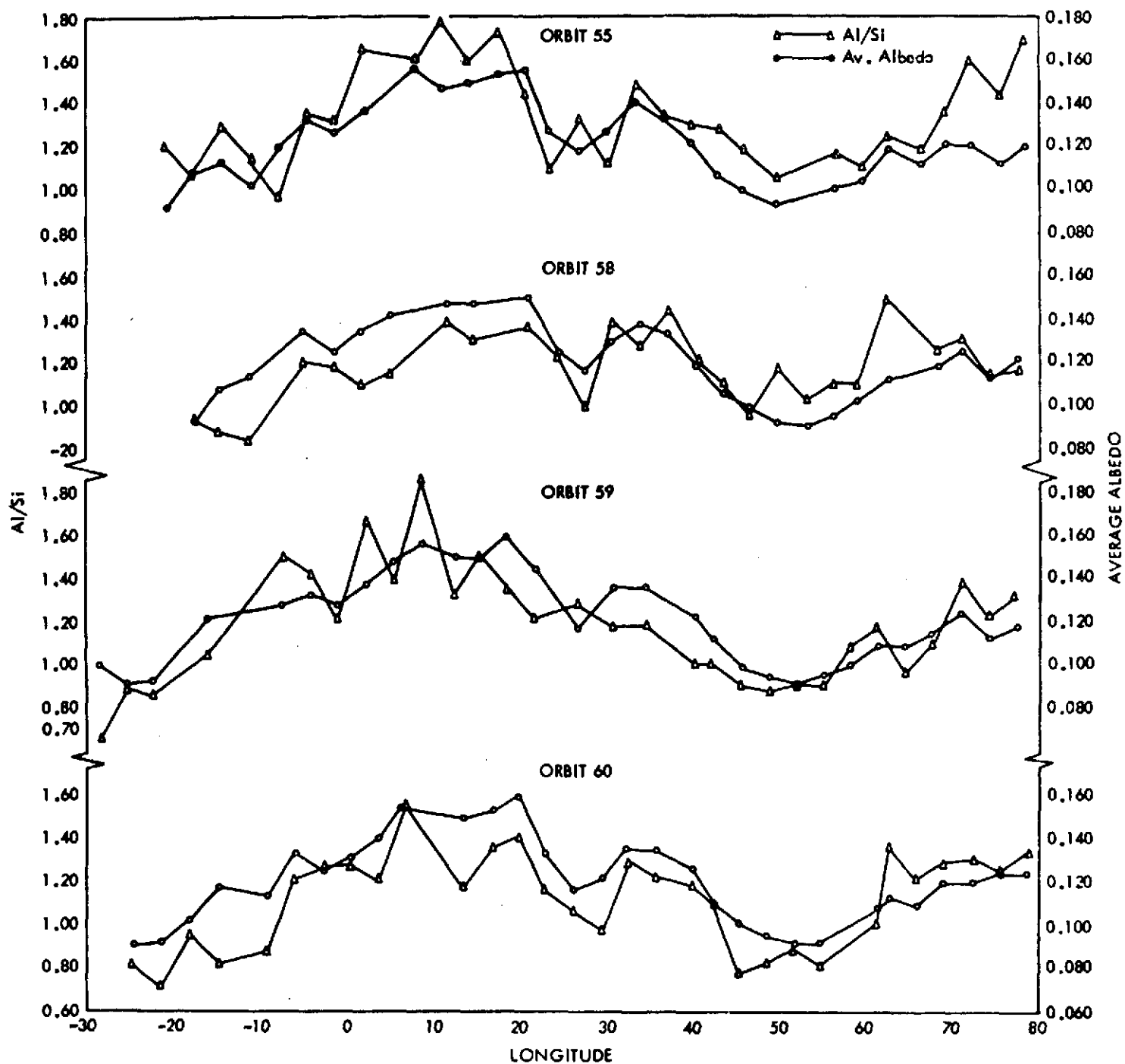
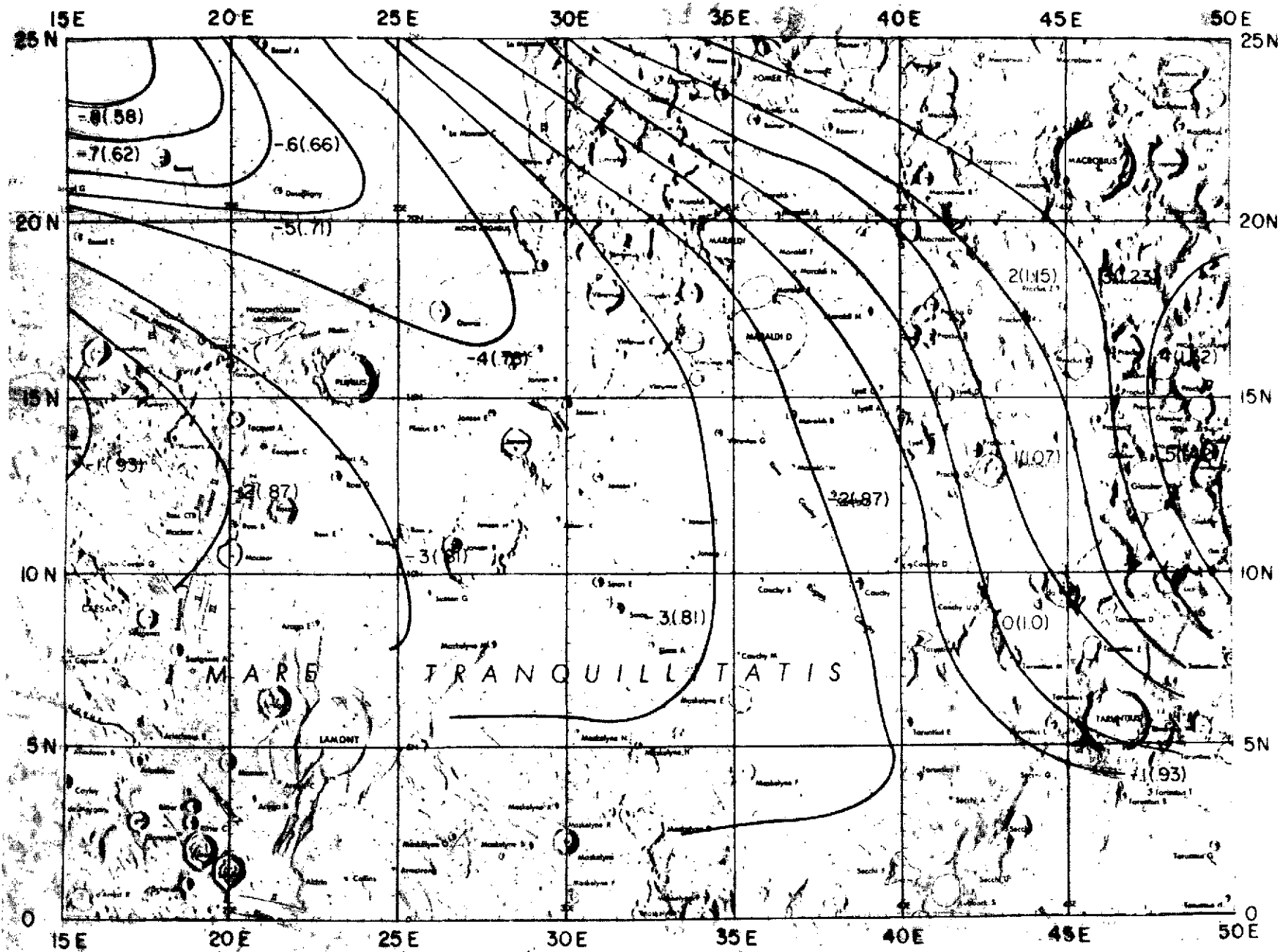


Figure 14.



FOURTH ORDER SURFACE
AI/Si-16 SECOND DATA

Figure 15.

